AD-A098 888 JAYCOR ALEXANDRIA VA F/G 20/9
TIME-DEPENDENT ION DIODE PHYSICS AND ION BEAM TRANSPORT IN STAB--ETC(U)
JAN 81 F L SANDEL N0013-79-C-0449
UNCLASSIFIED JAYCOR-PSD-200-81-001-FR NL

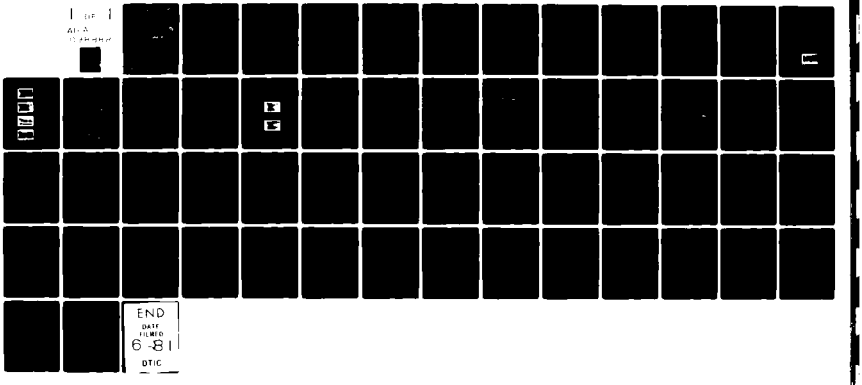

END
DATE FILMED
6-81
DTIC

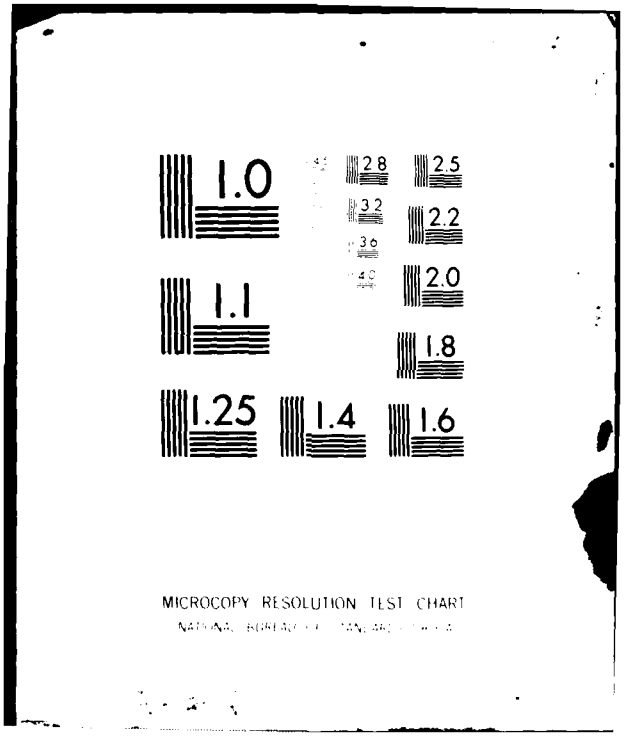
1.0
2.8
2.5
3.2
2.2
3.6
2.0
4.0
1.1
1.8
1.25
1.4
1.6
MICROCOPY RESOLUTION TEST CHART

LEVEL II

AD A098888

DTIC
ELECTE
MAY 13 1981
D

JAYCOR

DISTRIBUTION STATEMENT A
Approved for public release;
Distribution Unlimited

DTIC FILE COPY

205 South Whiting Street
Alexandria, Virginia 22304

81 5 12 026

TIME-DEPENDENT ION DIODE PHYSICS AND ION BEAM TRANSPORT IN STABILIZED PLASMA CHANNELS

JAYCOR Project 6173

JAYCOR Final Report No. PSD-200-81-001-FR
Contract No. N00173-79-C-0449

January 1981

Frederick L. Sandel

JAYCOR
205 S. Whiting Street
Alexandria, VA 22304

Submitted to:

Naval Research Laboratory
Washington, DC 20375

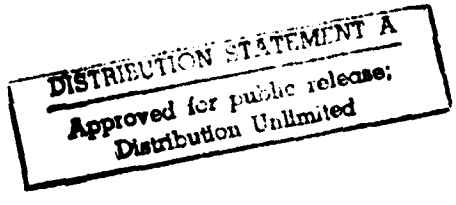

Unclassified

SECURITY CLASSIFICATION OF THIS PAGE (When Data Entered)

REPORT DOCUMENTATION PAGE	READ INSTRUCTIONS BEFORE COMPLETING FORM
1. REPORT NUMBER: PSD-200-81-001-FR	2. GOVT ACCESSION NO.: AD-A098 888	3. RECIPIENT'S CATALOG NUMBER:
4. TITLE (and Subtitle): Time-Dependent Ion Diode Physics and Ion Beam Transport in Stabilized Plasma Channels (6)	5. TYPE OF REPORT & PERIOD COVERED: Final Report 7/19/79 - 4/30/80
(14) JAYCOR	6. PERFORMING ORG. REPORT NUMBER: PSD-200-81-001-FR
7. AUTHOR(s): Frederick L. Sandel (10)	8. CONTRACT OR GRANT NUMBER(s): N00173-79-C-0449 (15)
9. PERFORMING ORGANIZATION NAME AND ADDRESS: JAYCOR, 205 South Whiting, Alexandria, VA 22304 (11) 31 Jan 81	10. PROGRAM ELEMENT, PROJECT, TASK AREA & WORK UNIT NUMBERS:
11. CONTROLLING OFFICE NAME AND ADDRESS: Naval Research Laboratory, Washington, DC 22375 (12) 55	12. REPORT DATE: January 31, 1981
	13. NUMBER OF PAGES: 54
14. MONITORING AGENCY NAME & ADDRESS (if different from Controlling Office): Same as block 11 (9) Final rept. 19 jul 79 - 30 apr 80	15. SECURITY CLASS. (of this report): Unclassified
	15a. DECLASSIFICATION/DOWNGRADING SCHEDULE:
16. DISTRIBUTION STATEMENT (of this Report): 1 copy - 4701; 1 copy - 4702; 1 copy - 4770; 1 copy - 2627; 2 copies - Defense Documentation Center	DISTRIBUTION STATEMENT A: Approved for public release; Distribution Unlimited
17. DISTRIBUTION STATEMENT (of the abstract entered in Block 20, if different from Report)	
18. SUPPLEMENTARY NOTES	
19. KEY WORDS (Continue on reverse side if necessary and identify by block number)	
20. ABSTRACT (Continue on reverse side if necessary and identify by block number)	

DD FORM 1 JAN 73 1473 EDITION OF 1 NOV 65 IS OBSOLETE
S/N 0102-LF-014-6601

993453

Unclassified

SECURITY CLASSIFICATION OF THIS PAGE (When Data Entered)

TIME-DEPENDENT ION DIODE PHYSICS AND ION BEAM TRANSPORT IN STABILIZED PLASMA CHANNELS

I. Introduction

This report summarizes work performed by JAYCOR which has led to significant advances in the understanding of ion diode physics as well as new knowledge of the processes of ion beam transport in the stabilized plasma channel systems previously developed by JAYCOR. The report is divided into three sections. Part A is a comprehensive study of the pinch-beam ion diode. This work was expanded considerably beyond the original scope of the contract and includes studies of anode materials, anode plasma behavior, time-dependent ion beam profiles, beam bunching, ion species and beam neutralization. Part B is a detailed analysis of plasma channel transport experiments in which previously unknown ion energy losses were discovered in the ion diode and/or focusing regions. This work was done in collaboration with S. A. Goldstein and P. G. Blauner of JAYCOR and F. C. Young, S. J. Stephanakis, G. Cooperstein and D. Mosher of NRL. Part C is a collection of abstracts of papers written during the period of this work.

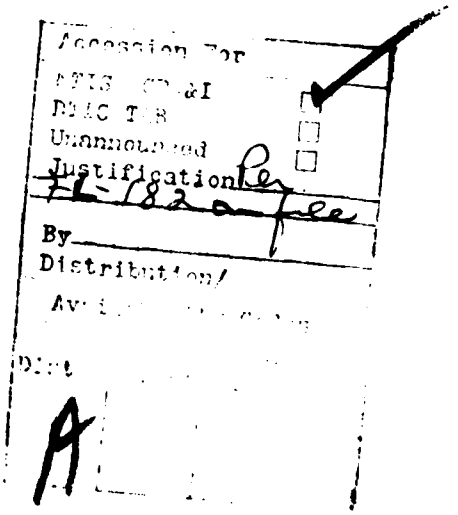

PART A

TIME-DEPENDENT ION DIODE PHYSICS

Previously JAYCOR has investigated the focussing and transport of light-ion beams produced in pinch-beam ion diodes on the NRL GAMBLE I accelerator. Of critical importance to the efficiency of the above processes is knowledge of the intrinsic characteristics of these diodes and the ion beams they produce. This report summarizes studies JAYCOR has made to investigate these characteristics.

First, the impedance behavior and ion generation in the diode is very sensitive to the composition and structure of the anode, which is the source of the ions. Also, the nature of the anode can affect the radial current distribution of the ion beam, filamentation and beam uniformity, and sharpness and reproducibility of a focus when curved focussing anodes are used. Furthermore, when the beam is propagated in a gas filled drift region, bulk current neutralization has been observed with a corresponding improvement in beam uniformity and filamentation. Finally, some anode structures allow the generation of ion beams under conditions where self-bunching of the beam is expected, allowing possible time-of-flight separation of ion species. These observations suggest continuing experiments which are in progress.

Figure 1 shows schematically the diode structures which are used to produce cylindrical and ballistically focussed ion beams. These diodes consist of a conducting anode which is pulsed positive, typically to one half megavolt, for a nominal 60 nanoseconds. The ion beam is extracted through a grounded cylindrical cathode of variable "hollowness". Various anode foils are the source of the ions, with possible ion production mechanisms being direct vaporization and ionization of the foil by electron deposition, flashover of the foil from charge accumulation, and u.v. ionization from the electron pinch.

PINCHED-BEAM ION DIODE

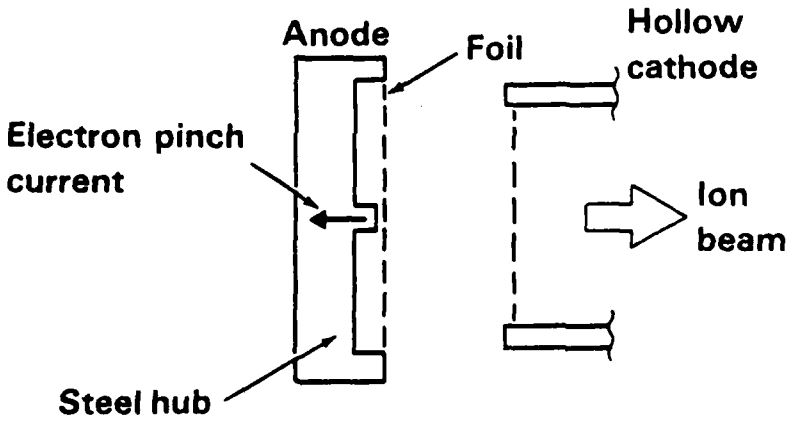

PLANAR

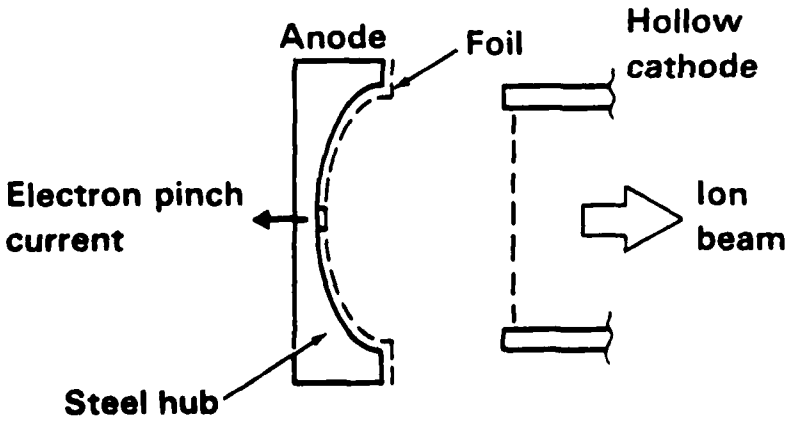

SPHERICAL (Focusing)

Figure 1

Figure 2 compares diode characteristics for various anode foils. For each anode, the corrected diode voltage, diode current, and impedance time history are shown, along with a biased probe measurement of the ion current pulse. For the case of a conducting 25 micron aluminum anode, flashover is eliminated as a possible ion generation mechanism, and the diode impedance history is a nearly monatonic decrease from high to low values during the pulse, with an abrupt impedance collapse phase at late times. The ion production occurs very late in the pulse as shown. When a 12.5 micron polyethylene anode is substituted, a similar impedance behavior is observed, but with a less dramatic collapse phase. However, the ion current begins much earlier in the pulse. Changing to a 75 micron mylar anode results in an early impedance collapse, but again the ion current begins early.

As shown in Figure 3, a 250 micron polyvinyl acetate, or PVA, anode gave a well controlled impedance history before a rather sharp collapse, as well as the earliest ion generation for the various solid foil anodes. However, a dramatic change in diode characteristics was observed when a 250 micron polyvinyl chloride or PVC coated fiberglas screen anode was used. This was suggested by Dave Johnson of Sandia Labs. The impedance fell to a low value very early in the pulse to a value half that of an identical diode with a solid plastic anode. The impedance remained remarkably constant during the pulse, sometimes even rising slightly as shown, and rarely exhibited a sharp impedance collapse. Ion production occurred earlier than in any other diode investigated.

These observations suggest a flashover mechanism may be more dominant in gridded anode structures than in solid anodes. Whenever possible, proton activation of carbon targets was compared to ion beam current measurements on each shot. In general, for solid plastic anodes, proton current was 50 to

IMPEDANCE CHARACTERISTICS AND ION PRODUCTION

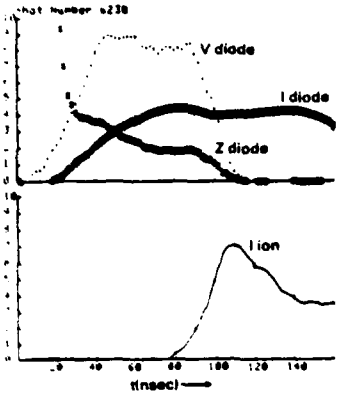

25 μm Al anode

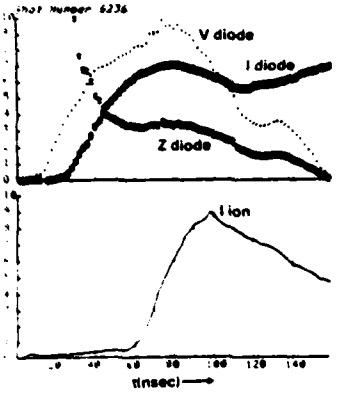

12.5 μm polyethylene anode

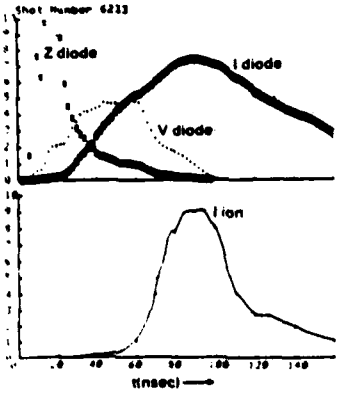

75 μm mylar anode

Figure 2

IMPEDANCE CHARACTERISTICS AND ION PRODUCTION

250 μm polyvinyl acetate (PVA) anode

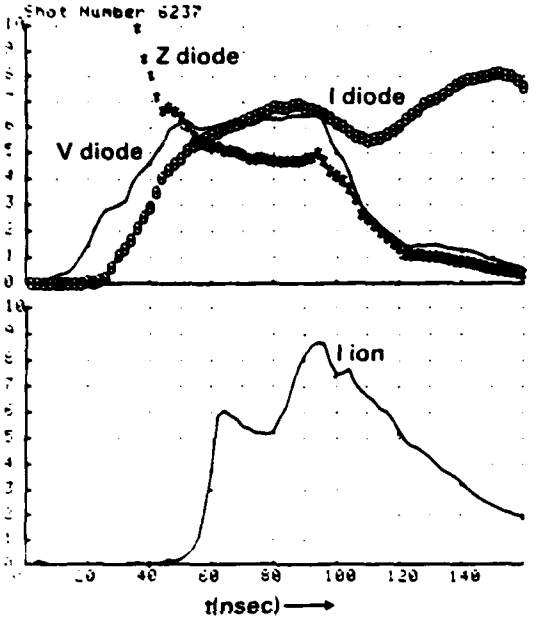

250 μm polyvinyl chloride (PVC) coated fiberglas screen

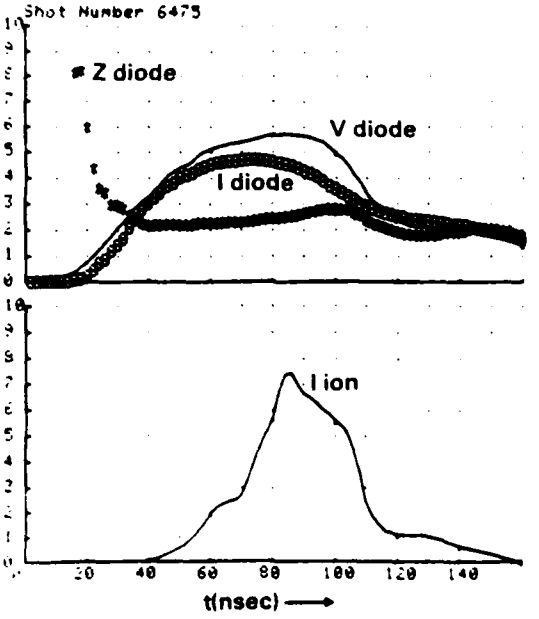

Figure 3

90 percent of the ion beam current, whereas for the gridded anodes inferred proton current was usually 50 percent or less of the total beam current. Also, the impedance behavior of the gridded anode suggests possible non-planar motion of the anode plasma expanding from the grid.

In an attempt to examine anode plasma behavior more directly, a window and collimation structure was made to allow a vertical strip across the anode diameter to be viewed with a streak camera at 23 degrees to the plane of the anode. (See Figure 4.) A 100 nanosecond streak photograph of the anode plasma light across the anode diameter is shown below.

Streak photographs of the anode plasma under various diode conditions are displayed in Figure 5. For the case of a solid PVA anode, light is emitted at large radii first and the emission progresses to the axis slowly over a period of 10 to 20 nanoseconds. The plasma shows some non-uniformities during the pulse. In contrast, the grid anode is seen to turn on almost instantaneously across the entire anode diameter, producing a very uniform plasma throughout the pulse. This again is a strong indication of a flash-over mechanism, whereas the PVA anode plasma suggests a turn-on associated with the collapsing pinch. The third streak photograph shows a PVA anode backed by a non-conducting hub, so that the pinch current is not forced into a symmetric flow. The non-uniformity and loss of beam centering is obvious. Finally, the last streak shows the anode plasma behavior when the cathode plane is intentionally made non-parallel to the anode plane. The asymmetric break-up of the plasma is apparent.

As a final test of the importance of flashover in the gridded anode, successive shots were taken with the anode grid acquadaged on the second shot to eliminate flashover. The analysis of these shots in Figure 6 points out

ANODE PLASMA BEHAVIOR

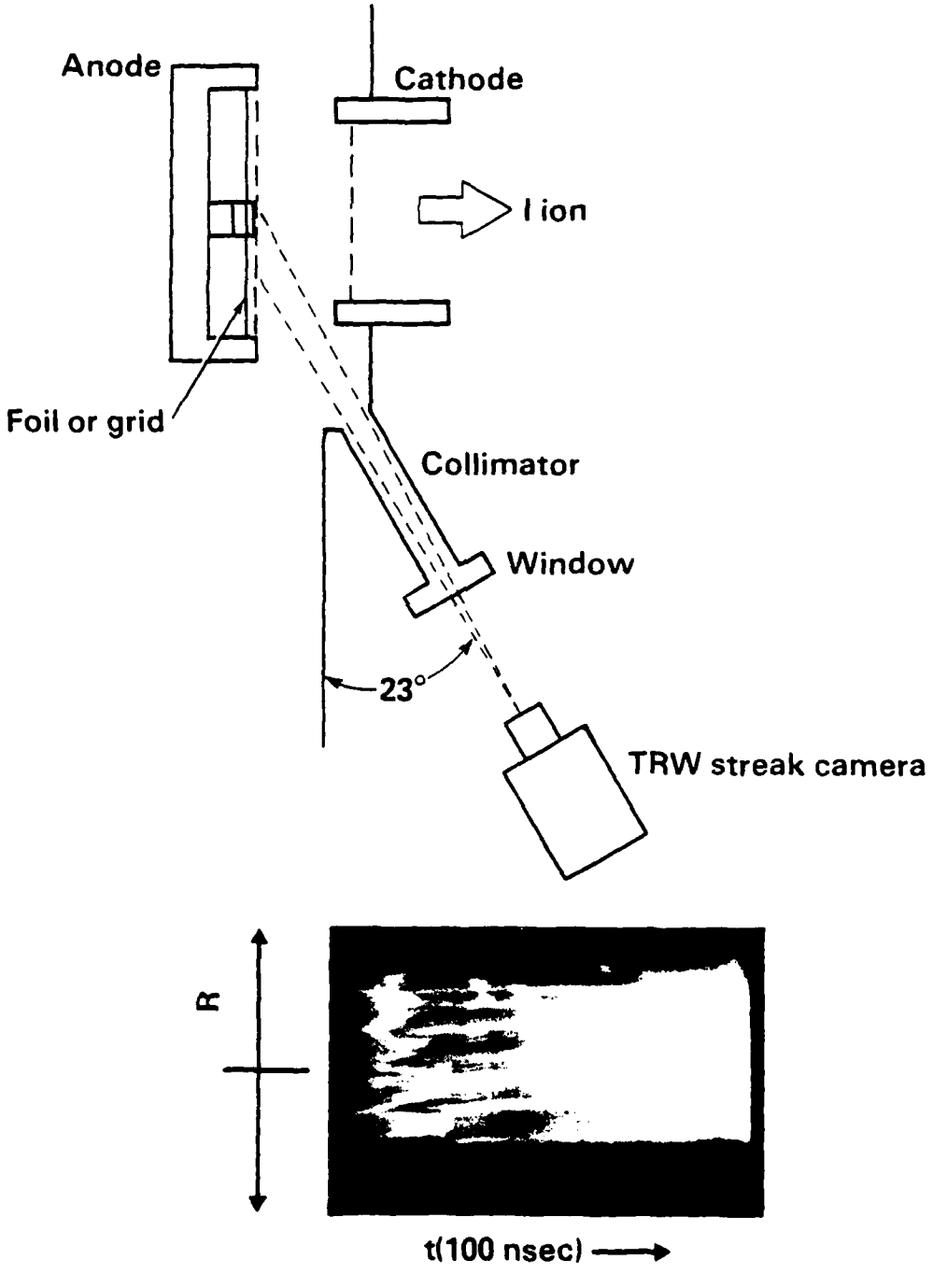

Figure 4

ANODE PLASMA BEHAVIOR

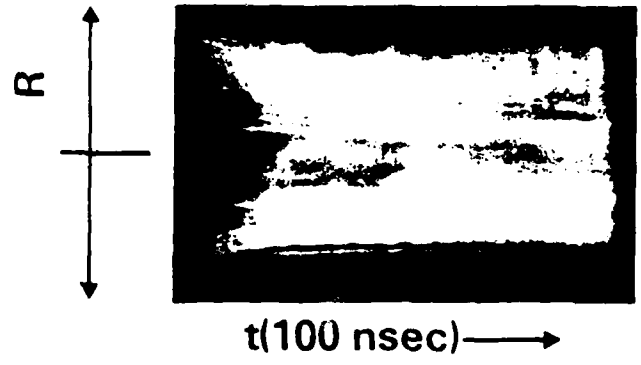

250 μm
polyvinyl acetate
anode (PVA)

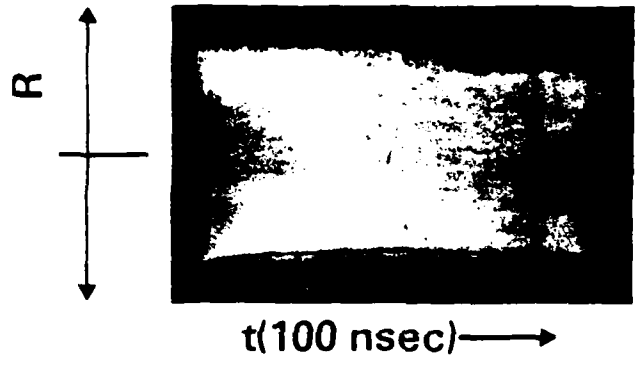

250 μm
PVC coated
fiberglas screen anode

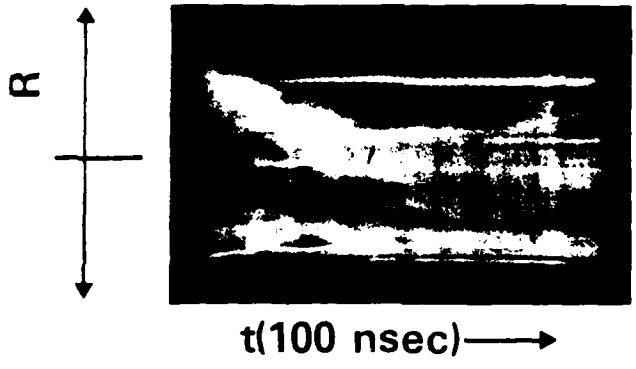

250 μm polyvinyl acetate
anode (backed with
dielectric hub)

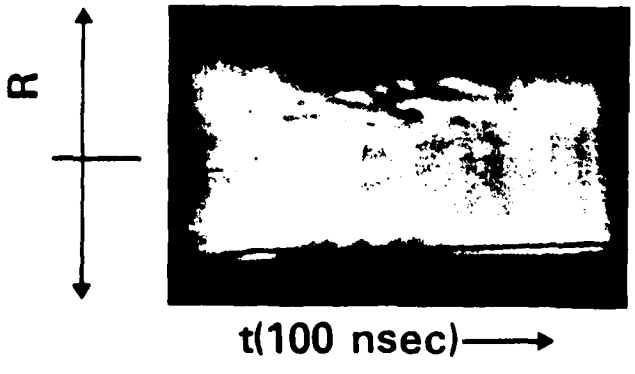

250 μm PVC coated
fiberglas screen anode
(cathode not parallel
to anode)

Figure 5

ANODE FLASHOVER

250 μm PVC coated fiberglas screen anode

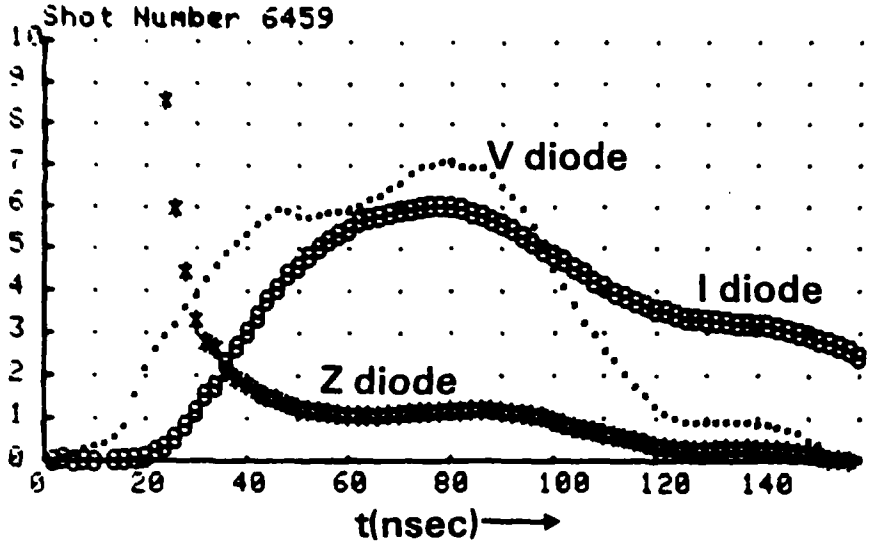

250 μm PVC coated fiberglas screen anode (coated with acquadag)

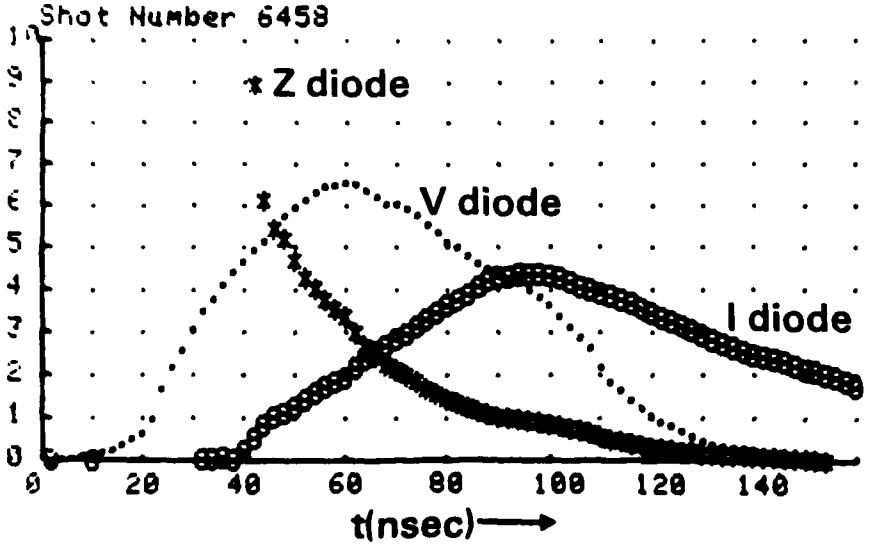

Figure 6

dramatic change in the impedance characteristic. With acquadag the impedance is a sharply decreasing function of time during the pulse as opposed to the rapid fall and constant impedance phase of the bare grid.

Measurements of the ion beam radial current profile with an array of biased collector probes 10 to 15 cm downstream of the diode showed evidence of hollowing of the beam during the pulse. As shown in Figure 7, an on-axis probe has peaked and is falling toward zero while a probe at a radius of 2 cm is reaching peak current. Furthermore, at the same time a probe at a radius of 3.5 cm is still rising toward peak current. One explanation of this might be self-focussing of the ion beam and a movement of the focus closer to the diode during the pulse. However, as Figure 8 suggests, occasionally there is evidence in the anode plasma streak photographs that we may be depleting the anode plasma late in the pulse. A dark region appears on the diode axis during the pulse and expands radially outward. This expansion velocity roughly corresponds to the rate of hollowing observed with the probe array.

Good current neutralization of the beam is necessary for injection of the ion beam into tranpsort systems. This was investigated using the experimental arrangement shown in Figure 9. The total net beam current was monitored with a fast current sensing coil and evidence that the beam was in fact present came from downstream activation targets and witness plates. A 2 micron kimfol inserted in the cathode allowed a differential pressure up to several Torr to be maintained in the drift region behind the cathode.

Figure 10 presents a typical ion current waveform as observed with a biased collector probe near the diode. This is compared with a typical net current waveshape observed when the beam passed through the gas filled drift region. The characteristic long decay time of the net current is apparent. As the curve at the bottom shows, merely passing the beam through the kimfol

ION BEAM RADIAL PROFILE

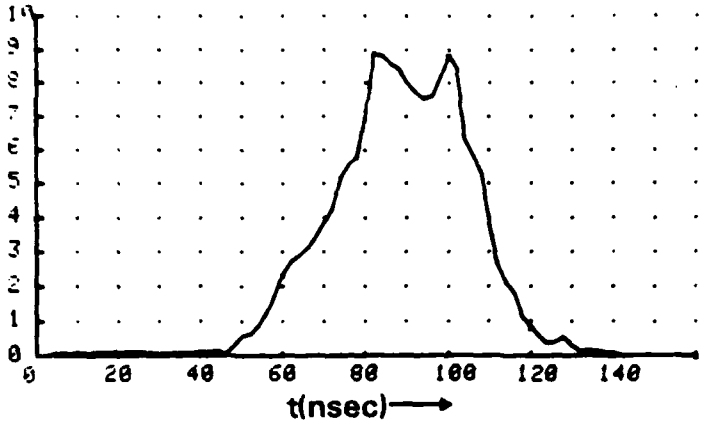

I ion
r=0 cm

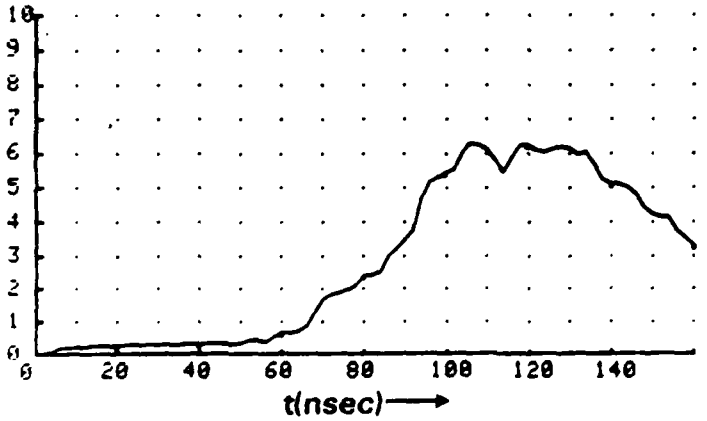

I ion
r=2 cm

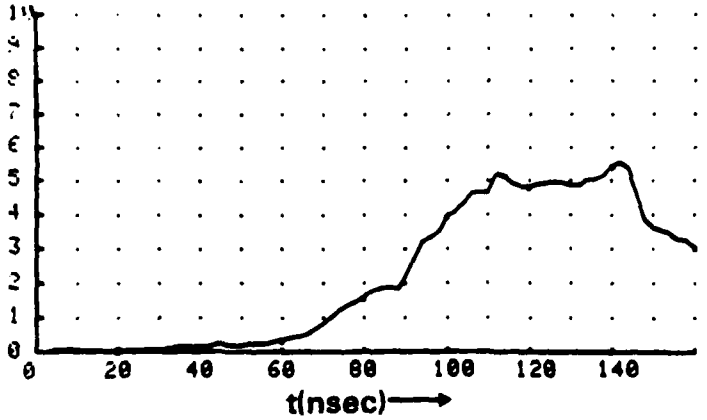

I ion
r=3.5 cm

Figure 7

POSSIBLE ANODE PLASMA DEPLETION

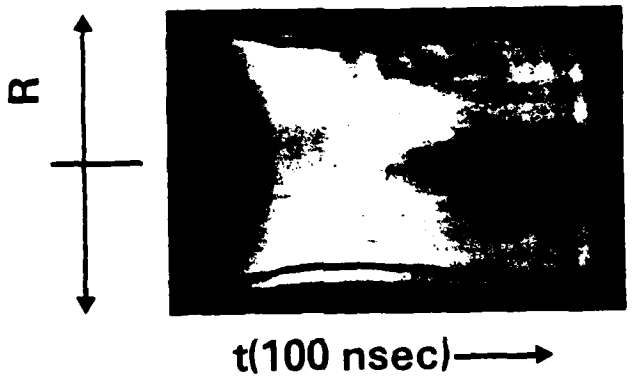

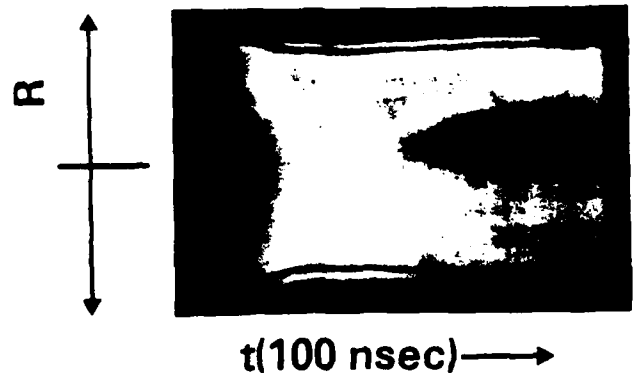

Figure 8

ION BEAM CURRENT NEUTRALIZATION

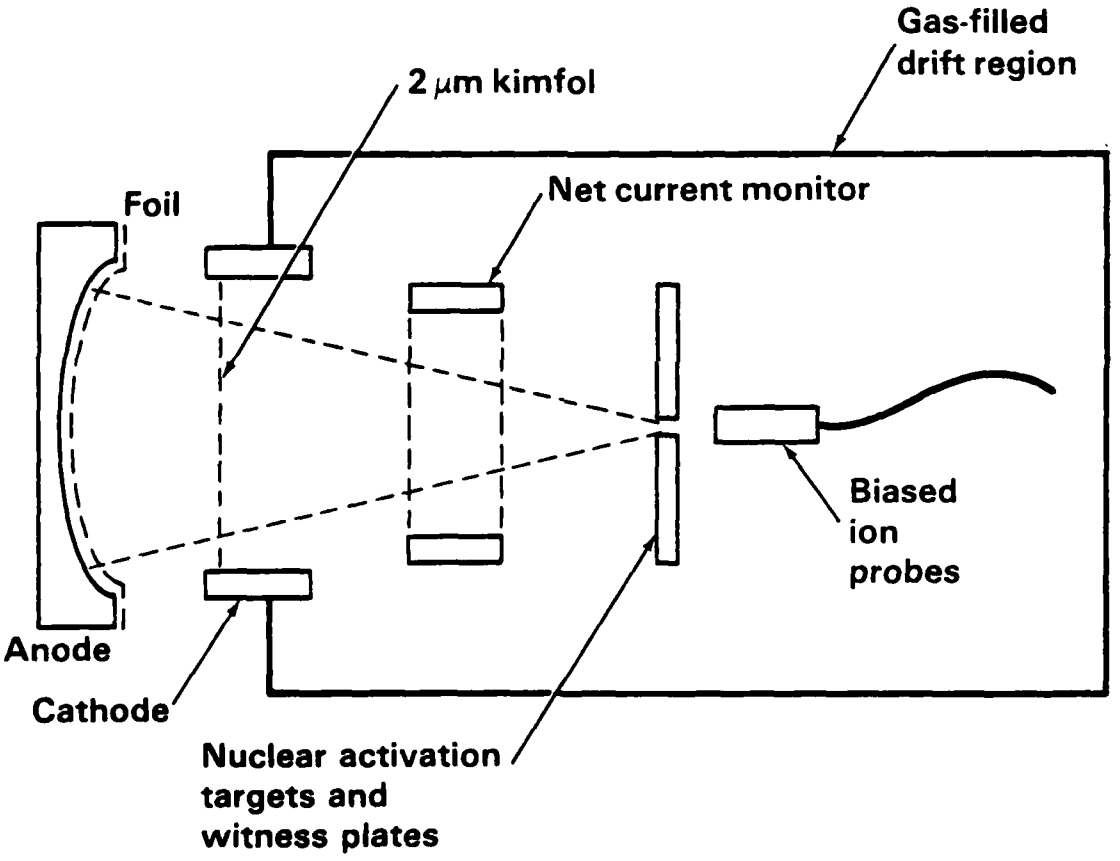

Figure 9

CURRENT NEUTRALIZATION

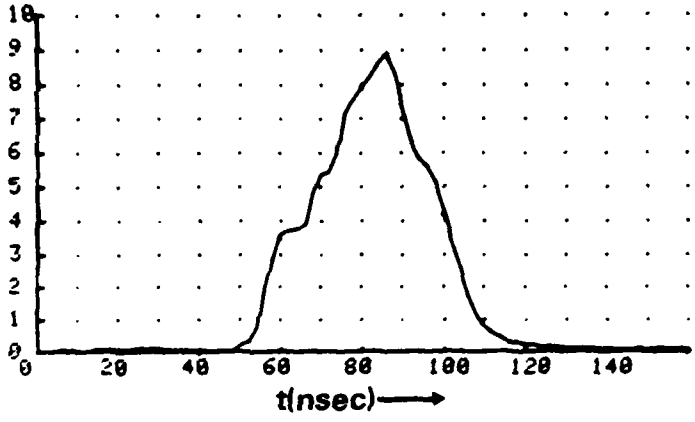

I ion

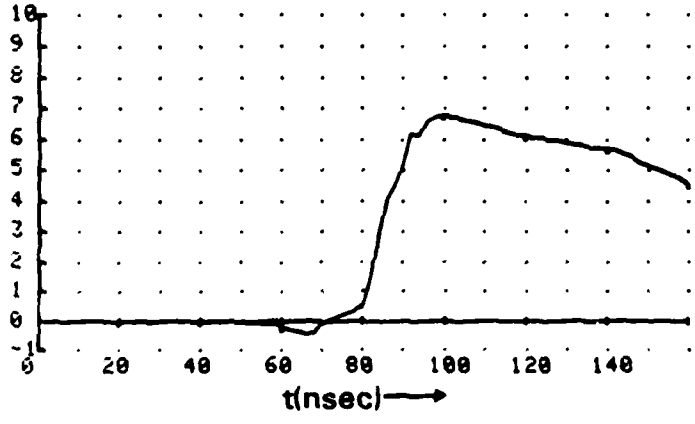

I net

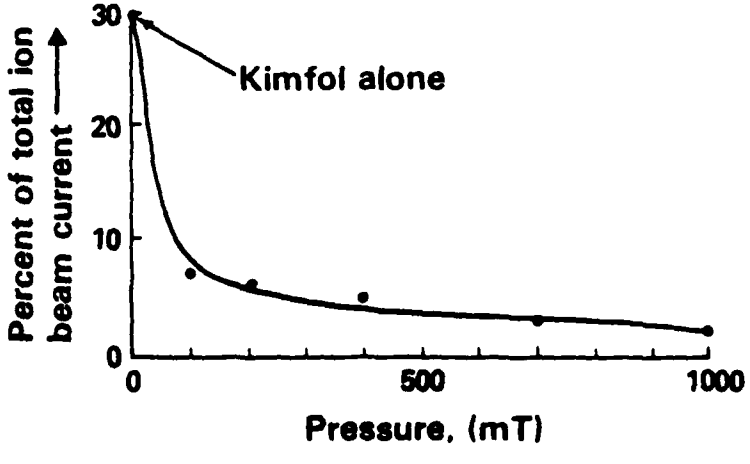

Figure 10

reduced the net current to 30 percent of its unneutralized value, although this reduction may be in part stopping of any heavy ion species, such as carbon. Then, as gas pressure behind the foil is increased, neutralization proceeds rapidly and at a pressure of 1 torr the beam is essentially current neutral. Examination of downstream aluminum witness plates with and without beam neutralization shows that neutralization improves focal spot centering when focussing anodes are used and greatly diminishes beam filamentation.

Returning again to the influence of the anode structure on the diode character, an interesting effect is apparent. Figure 11, where the diode wave forms for a solid PVA anode are compared to the PVC grid anode. In the case of PVA, the ions are typically produced later, and because of the time dependence of the impedance, in a falling diode voltage. However, because of the flashover and early fall of the impedance in the case of the grid, the ions are generally produced in a rising diode voltage, as shown on the lower figure. This opens the possibility of bunching of the beam as it propagates. Moreover, if the ion beam is multi-species, there is the possibility of time-of-flight separation of the species.

Ideally, considering Figure 12, one would want a diode voltage approaching that shown in the top figure, where the ion production occurs during a smooth voltage ramp. A simple arrangement was constructed to test for these effects as shown in the lower figure. The beam was sampled by a special probe 60 cm downstream from the diode. Fully non-current neutral or partially current neutral beams were used.

With a little finessing of the diode hardware and a liberal dose of dumb luck, it was possible to improve the diode voltage waveshape even more

DIODE VOLTAGE RAMPING FOR BUNCHING

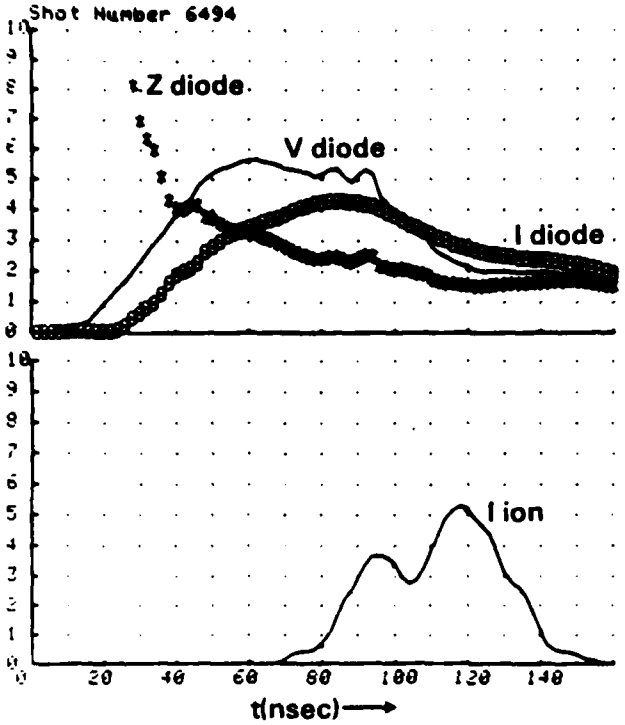

250 μm polyvinyl acetate (PVA) anode

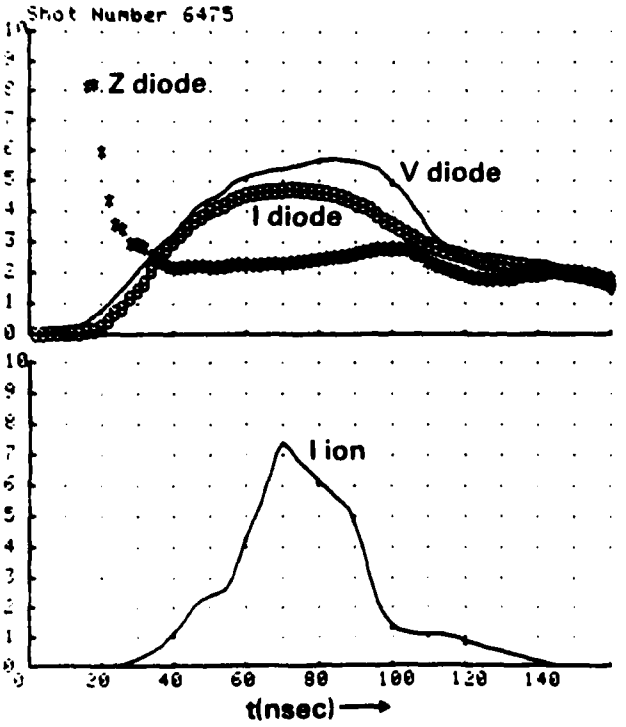

250 μm polyvinyl chloride (PVC) coated fiberglas screen anode

Figure 11

BUNCHING AND SEPARATION OF ION SPECIES

Idealized voltage pulse for bunching

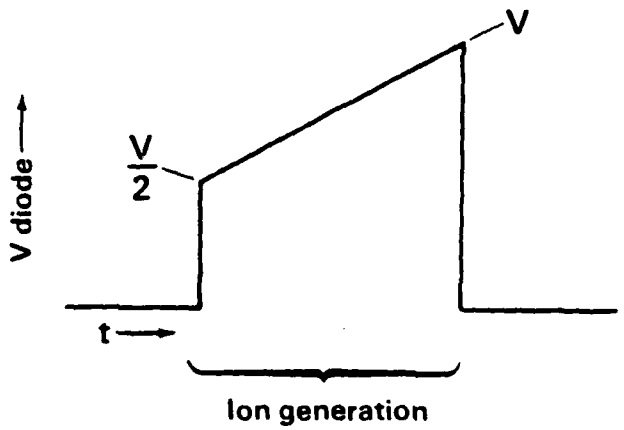

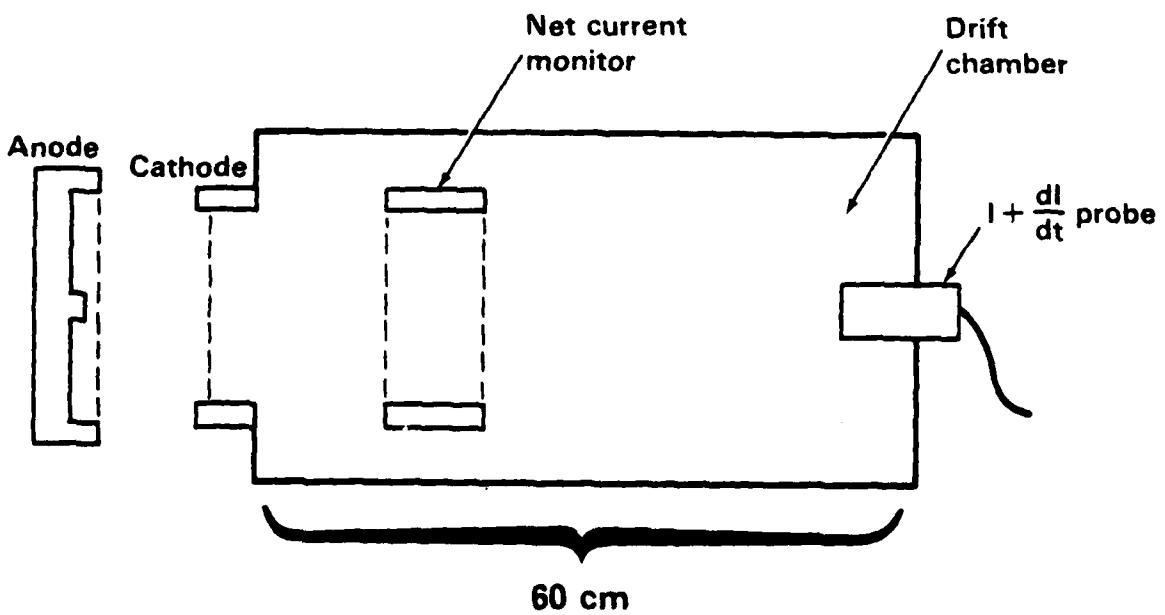

Figure 12

as shown in Figure 13. The voltage pulse now closely approximates the ideal waveshape.

Under these conditions, downstream ion current signals like the lower trace in Figure 14 are observed, as compared to the ion current near the diode which is typically as shown in the upper trace. Discrete peaks appear of approximately 10 nanoseconds full-width half-maximum. The species labels aligned with each peak show the species whose time of flight most closely fits the observed peaks. While this is certainly not a quantitative or definitive measurement, it is appealing to note that the trace suggests half or more of the beams produced by the gridded anode may be non-hydrogenic, which is consistent with the nuclear activations vs. total beam current measurements.

The preceding observations suggest several continuing experiments which are in progress. First, independent control of the ion species accelerated would be desirable, along with avoidance of anode plasma depletion. For these purposes an active anode using fast gas injection has been constructed. Also, so that various ion species may be identified in different diodes, a simple ion mass spectrometer is being constructed. Finally, new diodes utilizing mechanisms other than the pinched-beam process have been designed and built.

The gas-injection anode is shown schematically in Figure 15. The chosen gas is stored in a plenum and is delivered to a chamber in the rear of the anode by means of a timed fast electric valve. The gas equilibrates in the chamber and passes through a multi-layer diffuser, finally exponentially expanding into the anode-cathode region. The beam firing is timed so as to avoid gap short-out. A flashover screen may be included to assist in ionizing the gas. In addition to the advantages already mentioned, this type of diode holds out the possibility of repetitive pulsing. More advanced versions of this device will use external methods for preionizing the injected gas.

NEAR-IDEAL BUNCHING VOLTAGE PULSE

250 μm PVC coated fiberglas screen anode

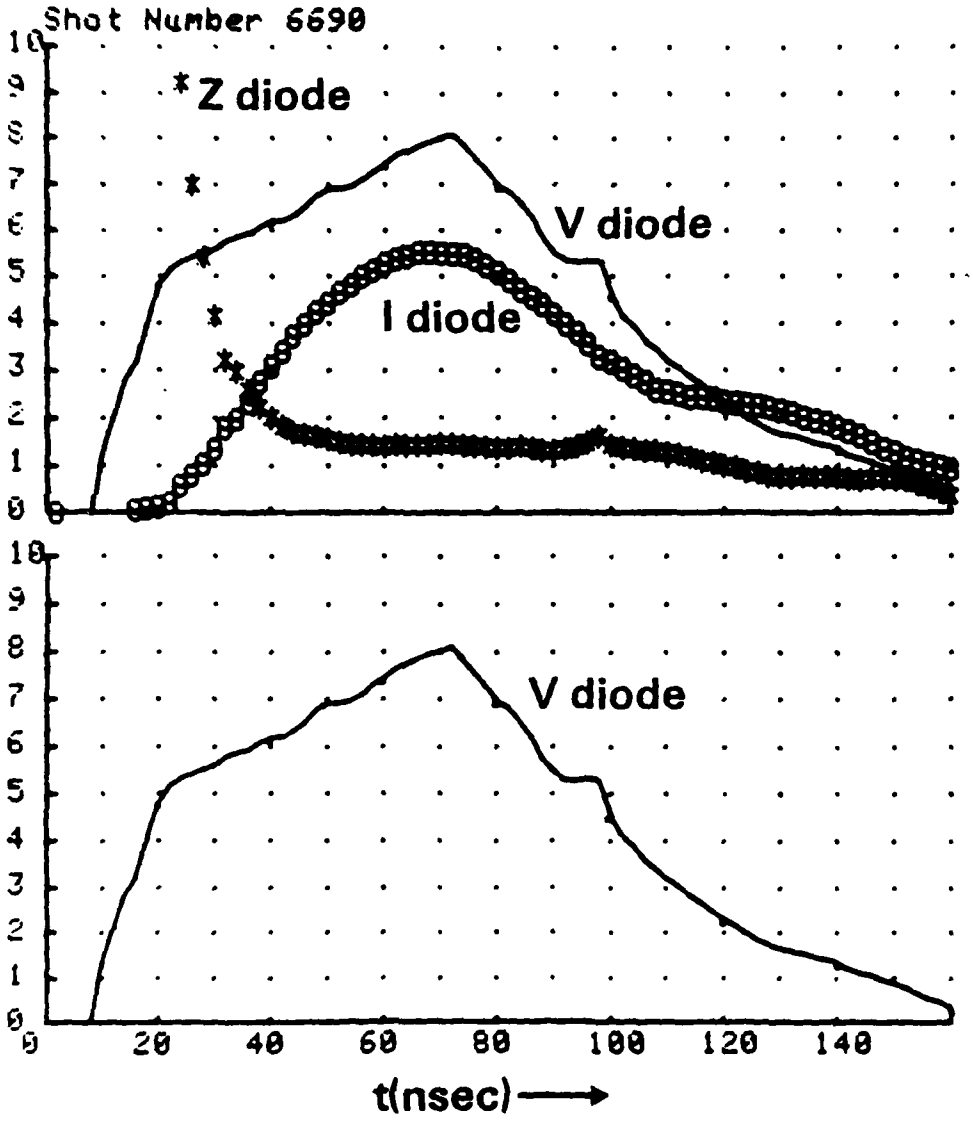

Figure 13

BUNCHED ION BEAM

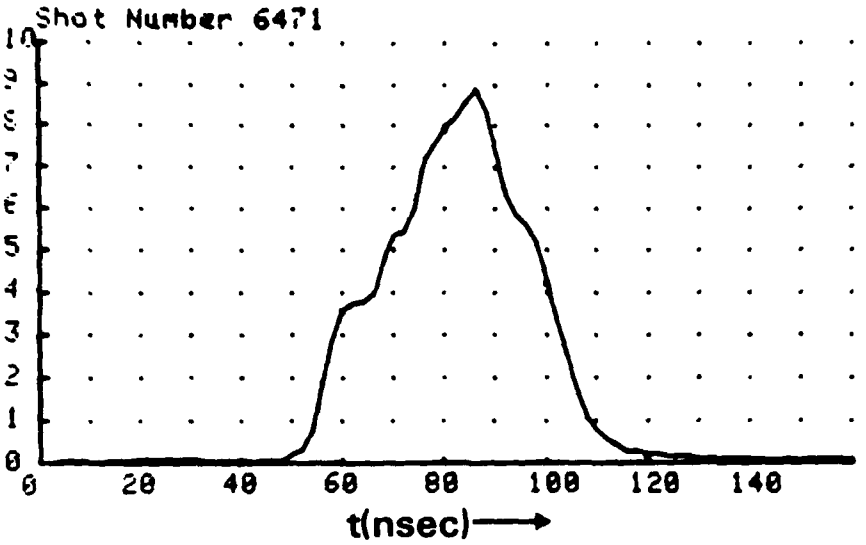

Typical I ion at diode

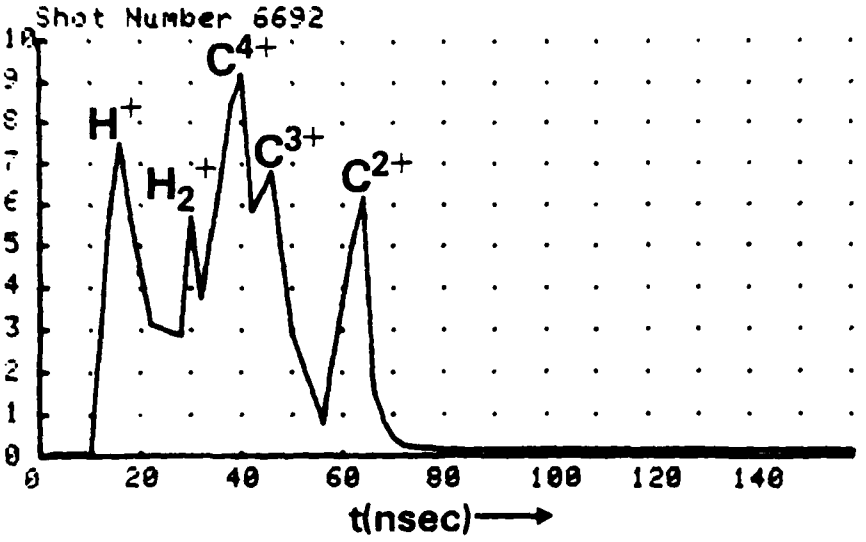

I ion at Z=60 cm

Figure 14

GAS INJECTION ANODE

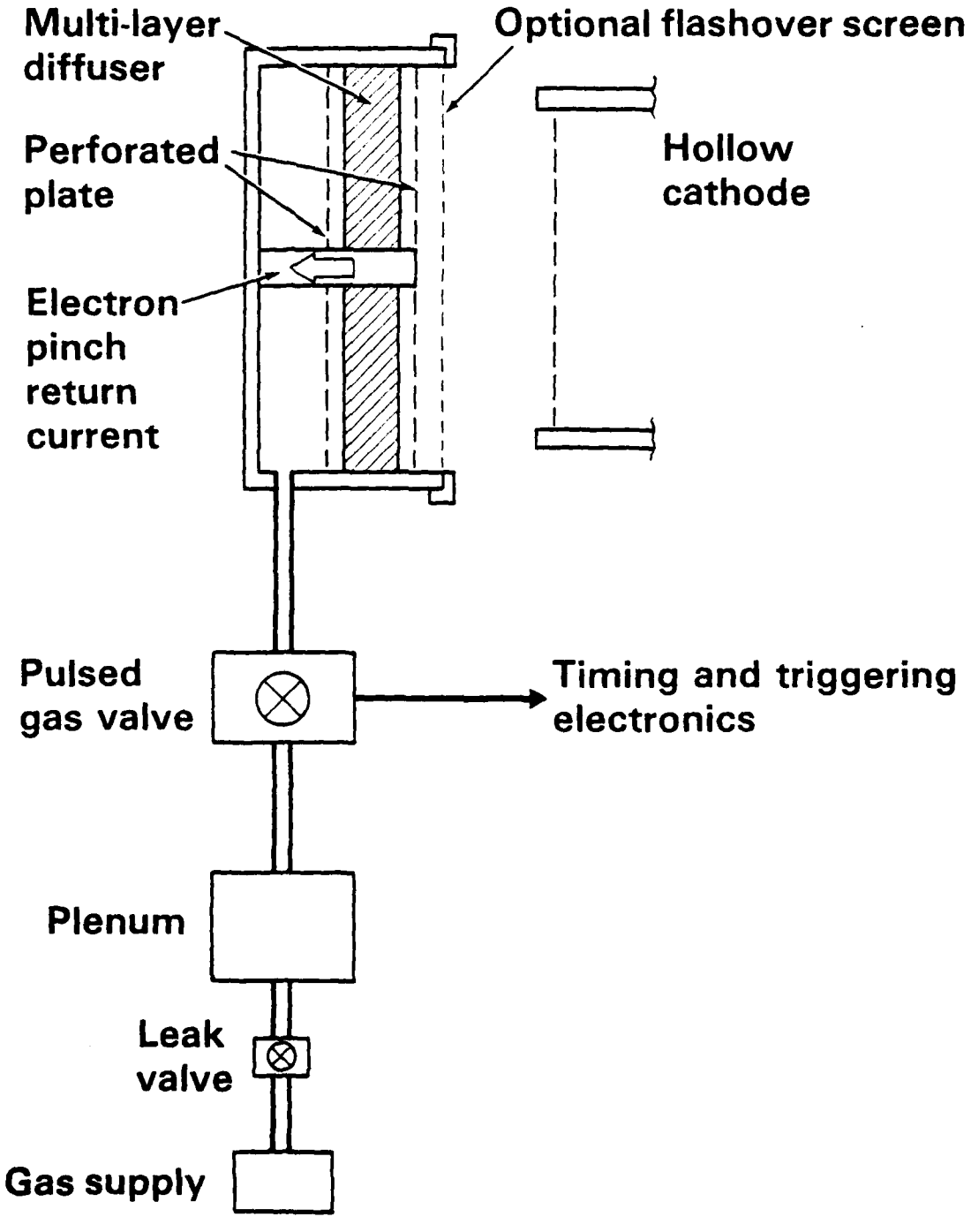

Figure 15.

PART B

ION BEAM TRANSPORT IN STABILIZED PLASMA CHANNELS

ANALYSIS OF PROTON TRANSPORT EXPERIMENTS

I. Introduction

As a part of the NRL light ion beam research program[1], experiments on the transport[2,3] of intense pulsed proton beams have been carried out. The NRL GAMBLE II pulser was used to generate proton beams and the measurement of prompt-gamma rays[4] was the primary diagnostic for proton transport. The first sequence of shots was made using a large-diameter (4.5 cm) transport channel with a 2.5-cm diameter aperture. The transport of 1-MeV proton beams of a few hundred kiloamperes a distance of one meter with efficiencies approaching 100% was achieved in this channel. A second sequence of shots with a smaller-diameter (1.6 cm) channel with a 1.2-cm diameter aperture was much less efficient in transporting the beam. Analysis of the prompt-gamma measurements to determine proton currents in the transport channel and transport efficiencies is presented in this report.

II. Description of Experiment

The proton beam was generated by a planar pinch-reflex diode[5] with a 5.7-cm radius cathode. The beam was brought to a narrow-angle focus 25 cm from the diode and injected into a transport channel. The vacuum diode was separated from the low-pressure-gas-filled transport region by a 1.8-μm thick Kimfol. The proton beam was focused by self B-fields in the 1.9-cm anode-to-Kimfol gap and, after passing through the Kimfol, was ballistically directed toward the focal region. At the expected focus, the beam entered the transport channel which consisted of a wall-stabilized plasma discharge

typically carrying an externally applied axial current of ∿ 50 kA. The B-field from this current was sufficient to confine the injected protons within the larger diameter channel.

The proton beam in the channel was diagnosed by measuring prompt gamma rays[4] from the $^{19}F(p,\alpha\gamma)^{16}O$ reaction. For this diagnostic, Teflon screen targets (50% transparent) were located at the entrance to the channel and one meter into the channel. Two detectors were used to measure prompt gamma rays from these targets as shown in Fig. 1. One detector, which was absolutely calibrated[6], was located 5ℓ cm from the second target and shielded against radiation from the diode and first target. The other detector was located behind a concrete wall and was equidistant from both targets. The wall differentially shields the diode bremsstrahlung and improves the signal-to-bremmstrahlung ratio for viewing the first target. Measured signals from these two detectors are displayed in Fig. 2. These responses indicate that the inside detector measured signals from the second target while the outside detector recorded signals from both targets. The outside-detector signals are separated in time by the transit of protons from the first to the second target. The detector behind the concrete wall was calibrated absolutely by comparing its response from the second target with that obtained with the inside detector.

For a shot with no Teflon targets, the prompt-gamma responses are given by the dashed curves in Fig. 2. On this background shot, sufficient energy was transported to spall an aluminum plate at the end of the transport system. A small bremsstrahlung signal was measured on the outside detector. The inside detector recorded no bremsstrahlung but did record a small signal probably due to residual Teflon deposited in the transport system from

previous shots. If the apparatus was not cleaned carefully between shots, this background was significantly larger.

Protons injected into the transport channel propagate in the magnetic field associated with the discharge current. The channel is essentially a z-pinch, a radial implosion followed by damped radial oscillations. The confinement of the protons to the channel depends on the radial profiles of the magnetic field, current, and particle density in the channel. These qualities are rapidly varying functions of time and are not known. For the present analysis, the channel is assumed to be of uniform particle and current density and constant in time for the duration of the beam pulse.

Measured prompt-gamma responses were compared to responses calculated using the ion current and proton energy measured on each shot. The charged-particle current incident on the Kimfol was measured with a Rogowski coil. The proton energy was taken to be the voltage determined by correcting the measured diode voltage for inductive effects in the diode and for classical energy loss in the Kimfol. The ion current, presumed to be entirely protons, and the proton energy were combined with the energy dependence of the $^{19}F(p,\alpha\gamma)^{16}O$ reaction and the absolute detector sensitivity[6] to give the expected prompt-gamma response. The energy dependence of this reaction yield is shown in Fig. 3. Corrections for the flight time of protons from the anode to the target were included in the calculations. The shapes and magnitudes of the calculated responses were compared to the measured responses after timing-chain corrections.

III. Large-Transport-Channel Results

Six shots with the large-diameter transport channel were selected for careful analysis. The calculated prompt-gamma responses for these shots are compared with the measured signals in Fig. 4. Here the calculated responses

have been normalized in amplitude to the measured signals. The proton current and energy used for these calculations are also displayed in Fig. 4 for each shot. The current measured on shot 407 was used for shot 406 because that trace was not recorded on shot 406.

The shapes of the calculated responses from the first target agree reasonably well with the measured traces for all the shots except shot 413. Also, the calculated risetimes for responses from the first target agree with the measured traces except for shot 402. The prompt-gamma signals from the first target for shots 402 and 403 were measured at 50 ns/cm and expanded to 20 ns/cm for the comparison in the attached figures. An error of ± 5 ns is inherent in the absolute time scale for these two traces. For shot 413, the calculated response from the first target is narrower in width than the measured trace. The calculated response is narrowed in time due to the peculiar shape of the voltage trace measured on this shot. The narrow peak on the prompt-gamma response is correlated with the narrow peak at the top of the voltage. Explanations for the discrepancy with the measured trace are speculated upon in the discussion (Section VI).

The calculated responses from the second target do not agree with the measured signals in shape or timing. The calculated responses occur too early in time presumably because the proton energy is too high. No energy loss in the focusing region or the transport system has been included in these calculations.

IV. Transport Efficiencies and Energy Losses in the Large Channel

A lower limit on the transport efficiency can be estimated from the ratio of the prompt-gamma signals from the first and second targets. Signals from both targets are recorded with equal sensitivity by the outside detector. The areas of the two peaks in the traces for this detector were used to

evaluate the transport efficiencies given in Table 1. For this evaluation the area of the second peak has been doubled relative to the first peak to correct for the 50% transparent Teflon screen targets. Table 1 also lists the air pressure in the transport channel for each shot. The largest transport efficiency was obtained for 0.5-Torr pressure. At a pressure of 0.12 Torr, the efficiency was reduced to about 20%. These efficiencies are in fact lower limits on the transport efficiency because energy lost by protons in the transport system causes the prompt-gamma signal from the second target to be reduced. The strong energy dependence of this diagnostic is shown in Fig. 3.

To estimate the magnitude of energy losses in these experiments, the average energy of the protons in the transport channel was determined for several shots. The time interval between signals from the two Teflon targets was used to calculate the average proton energy, E_a, in the channel. This energy is compared in Table 2 with the maximum energy of the ions, E_m, after passing through the Kimfol. The difference between E_m and E_a represents an average energy loss and ranges from 100 to 430 keV for these shots. For this comparison, a proton energy extracted from the timing of the maxima of the prompt-gamma responses should correspond to the peak proton energy because this response is strongly energy dependent (see Fig. 3). The average energy losses in Table 2 are larger than one expects from collisional losses in the channel. For example, the classical energy loss for 1.2-MeV protons in 1.5-Torr air is only 50 keV/m. Classical energy losses from the Kimfol to the second target due to the low pressure air in the channel are listed as dE_2 in Table 2. Clearly, energy losses significantly greater than classical collisional losses are reducing the proton energy in these experiments.

Table 1

Large-Channel Transport Results for No Energy Loss

Shot No.	Transport Channel Pressure (Torr)	Minimum Transport Efficiency
402	1.5	0.25
403	1.5	0.12
406	1.5	0.30
407	1.5	0.26
412	0.5	0.47
413	0.28	0.31

Table 2

Energy Loss Estimates

Shot No.	E_m (MeV)	E_a (MeV)	Average Energy Loss (keV)	dE_2 (keV)	ΔE_2 (keV)	dE_1 (keV)
402	0.975	0.88	100	70	300	13
403	1.10	0.93	170	60	--	--
406	1.22	0.96	260	64	--	--
407	1.39	1.01	380	60	600	12
412	1.26	0.93	330	21	500	4
413	1.44	1.01	430	10	700	2

An evaluation of the transport efficiency including energy loss was made for shots 402, 407, 412 and 413. On these shots, efficient transport was observed and all data traces were obtained. For this analysis, the energy loss was assumed to be constant during the beam pulse and was applied directly to the measured voltage to reduce the energy of the protons before time-of-flight corrections thru the focusing and transport sections. The energy loss of the protons after passing through the Kimfol was assumed to consist of a classical energy loss dE due to gas in the channel, and an additional energy loss ΔE to be determined. Subscripts of 1 or 2 will be used on these quantites to denote energy losses from the diode to the first or second Teflon target, respectively. The energy loss of protons from the diode to the Teflon target at the end of the transport system was determined from proton time-of-flight. The energy of the protons after passing through the Kimfol was reduced about an amount $(dE_2 + \Delta E_2)$, and ΔE_2 was adjusted so that the peak of the calculated prompt-gamma signal from the second target agreed in time with the measured signal. Values of dE_2 and ΔE_2 are given in Table 2. An uncertainty of ± 100 keV is assigned to ΔE_2 based on this fitting procedure. The fitting procedure is illustrated in Fig. 6. In all cases the additional energy loss ΔE_2 is much greater than the classical energy loss dE_2. The energy of protons striking the second target is less than the average energy measured in the transport channel, assuming deceleration during transport. Therefore the energy loss from the Kimfol to the second target is larger than the average-energy-loss estimates in Table 2.

The energy loss of the protons is made up of an energy loss in the region from the diode to the first Teflon target (ΔE_1), and an energy loss in the transport channel between the two targets (ΔE_t), where $\Delta E_1 + \Delta E_t = \Delta E_2$. Both ΔE_1 and ΔE_t are not known, but the sum, ΔE_2, was determined above.

A range of values for ΔE_t (and hence ΔE_1) is determined by comparing the intensities of measured and calculated prompt-gamma responses. Prompt-gamma responses were calculated for the first target with protons reduced in energy by $(dE_1 + \Delta E_1)$ and for the second target with protons reduced in energy by $(dE_2 + \Delta E_2)$. The ratio for these results was used to correct the minimum transport efficiencies determined previously for no energy loss. The results are presented in Fig. 5 as a function of ΔE_t. Values of dE_1 are given in Table 2. As ΔE_t increases, the transport efficiency increases until an upper-limit of 100% is reached. Over this range, ΔE_t never exceeds 150 keV and is always less than ΔE_1. For ΔE_t = 100 keV, a likely value, the transport efficiency ranges from 50% to 90%, and ΔE_1 ranges from 200 to 600 keV for these shots.

Only a fraction of the measured ion current is incident on the 2.5-cm diameter Teflon target at the entrance to the transport channel. The fraction of the ion current required to fit the magnitude of the measured prompt-gamma signal from the first target is determined by scaling the measured ion current by the ratio of the measured to calculated prompt-gamma signals. This fraction was determined by integrating the respective signals to eliminate uncertainties due to proton bunching and multiplying by two to correct for the 50% transmission Teflon screen target. This fraction is presented in Fig. 5 as a function of the energy loss in the transport channel, ΔE_t. For less energy loss in the transport channel and more energy loss from the diode to the channel entrance, a larger fraction of the ion current is required to account for the magnitude of the prompt-gamma signal. For ΔE_t = 100 keV, this fraction ranges from 20% to 85% for these shots. Since the measured ion current at peak voltage is about 500 kA for all these

shots (see Fig. 1), currents of 100 to 400 kA at peak voltage were inferred from this analysis.

The inclusion of energy losses in calculating the prompt-gamma responses has minimal effect on the shapes of the calculated responses as illustrated in Fig. 6 for shot 412. The fitting procedure used to determine the energy loss ΔE_2 is shown for the inside detector. If this same energy loss is used for ΔE_1 (i.e. $\Delta E_t = 0$), the timing of the calculated signal from the first target is only slightly delayed because the flight path of protons to the first target is so short.

V. Small-Transport-Channel Results

Measured prompt-gamma signals for two shots with protons injected into the small-diameter transport channel are compared with calculated responses in Fig. 7. These shots were selected because they gave observable transport. Other shots gave unobservable or barely observable transport. The reason for the poor transport in these shots will be discussed later. The proton energy and current used for these calculations are also displayed in Fig. 7. No energy losses have been included in the calculations, and the calculated responses were normalized in amplitude to the measured signals. For shot 419, helium gas was used in the channel instead of air. The channel pressure for each shot is given in Table 3.

The shapes of the calculated responses from the first target compare favorably with the measured traces, but the measured traces occur significantly earlier than the calculated traces. This discrepancy is due to a significant contribution to the first-target signal from diode bremmstrahlung. The measured signals are smaller due to the smaller entrance aperture on the transport channel, and the diode bremsstrahlung is larger in this series of shots so the signal-to-bremsstrahlung ratio is reduced.

The calculated responses from the second target do not agree with the measured signals in shape or absolute time. In fact, for shot 419 the measured response occurs earlier in the time than the calculated response. This suggests that the energy of some protons is greater than the measured diode voltage so that they arrive at the second target earlier in time. One might suspect that this early-time signal is due to protons bombarding a Teflon deposit remaining on the inside walls of the transport channel after previous shots. However, this explanation is unlikely because the channel was carefully cleaned between shots (see Fig. 2).

An analysis including energy loss has not been applied to these small transport channel shots because there are unknown bremsstrahlung contributions to the prompt-gamma signals from the first target and because the proton energy loss from the diode to the second target is poorly determined. Even so, minimum transport efficiencies may be evaluated from the ratio of the measured prompt-gamma signals from the two targets. The results are given in Table 3. These efficiencies are significantly smaller than the results obtained with the larger diameter channel.

Table 3

Small-Channel Transport Results for No Energy Loss

Shot No.	Gas	Transport Channel Pressure (Torr)	Minimum Transport Efficiency
417	Air	0.25	0.06
419	He	1.0	0.09

VI. Discussion

Protons injected into the transport channel propagate in and are confined by the magnetic field produced by the discharge current. Confinement within the channel depends on many factors. If a uniform static discharge current, I, is assumed, then protons entering the channel at angles up to a maximum of θ_m to the channel axis will be confined according to[3]

$$I = \frac{10^{-3}v(1-\cos\theta_m)}{1-(a/R)^2}$$

where I is in amperes, v is the proton speed in cm/s, R is the channel radius and $a < R$ is the radius of the channel entrance aperture. For 1-MeV protons and the maximum possible injection angle in the present experiments, a current of 58 kA in the large channel or 72 kA in the small channel is required.

In the experiments, typically 50 to 60 kA flowed in the large channel, but only $\sim$ 30 kA flowed in the small channel due to the increased channel resistance and the capacitor bank limitations. In the latter case, the channel current quarter-period rise time was about 15 μs. It is tempting to conclude that the transport efficiencies observed in the small channel were determined principally by the available discharge current. However, it was found in the experiments that observable transport ceased at the highest current levels in the small channel. Transport efficiency was increased by injecting the beam earlier in the rise of the channel current or by shortening the rise time of the channel current, even though the absolute level of channel current decreased.

These observations point to the necessity for a more realistic interpretation of the beam-channel system. The radial profiles of magnetic field, current, and density in the channel are rapidly varying functions of time and depend on such variables as plasma temperature, gas composition, impurity

contamination from the channel walls, etc. Thus, the transport efficiency depends on a detailed knowledge of the channel properties at the moment of beam injection and of the interaction of the beam-plasma system. We cannot presently obtain this information experimentally because the discharge is difficult to probe without disruption which may effect beam transport. MHD code work simulating the beam-discharge interaction is in progress.[7] For some channel conditions, MHD instabilities, which can inhibit transport, may grow.[8] The abrupt loss of transport at higher currents in the small channel suggests this possibility. Future experiments will test the role of instabilities by establishing the channel current on a much faster time scale. Under this condition, the instability growth time before beam injection is reduced.

The observed beam-energy losses cannot be simply explained at present. The results indicate that the energy losses substantially exceed those expected from classical collisional losses in the gas at fill pressure. It is apparent that losses occur both in the region between the anode and the transport channel entrance aperture and within the channel itself. In many cases, the out-of-channel losses are more severe. There are many possible explanations for these losses. In the pinch-reflex diode, the anode foil is vaporized and ionized to some extent by the electron beam. The electrons reflex through this plasma on their way to the pinch region at the anode center. This is a resistive plasma so that a substantial radial voltage drop can occur across this plasma. The energy of ions extracted from this plasma would depend on their point of origin within the plasma and would always be less than or equal to the voltage applied to the diode. Also, the self-inductance of the beam between the anode and the Kimfol extracts energy from the beam. Additionally, there may be losses due to microturbulence in the

gas,[8] and associated losses due to resistive and hydrodynamic electric fields which develop inside the channel during beam transport.[7] Furthermore, since a dynamic plasma exists in the transport system, the beam may lose or gain energy from axial electric fields created from plasma contraction or expansion.[9] This may explain the apparent acceleration of some protons to energies greater than the diode voltage as observed on shot 419. Finally, ions confined to a region close to the axis of the transport channel may sustain enhanced collisional losses if the pinch has compressed the plasma to densities significantly greater than the fill pressure. Wall material brought into the discharge during implosion can also contribute to collisional losses.

The large-diameter-channel measurements indicate that most of the ion beam could be injected into the 2.5-cm diameter aperture and transported. For the small channel, measurements from the first target indicate that less than half of the proton beam is contained within the 1.2-cm diameter aperture. On some shots with the small transport channel, the entrance aperture was increased to 1.6-cm diameter and the first target was removed. Signals from the second target increased by more than the factor-of-two expected by just removing the 50% transmission target. In this case, more protons were injected into the channel and transported. It should be noted that since the voltage and current of the ion beam vary in time, the position of best focus moves axially during the beam pulse. For inertial confinement fusion applications, diodes with improved focusability at long focal lengths are required.[3]

In the large-transport-channel analysis (Section IV), energy losses from the diode to the transport channel and within the channel itself were assumed constant during the beam pulse. For the reasons described above, it is apparent that the energy loss is not constant. Therefore, it is not

surprising that the shapes of the calculated prompt-gamma responses do not fit the shapes of the measured signals from the second target even though time-of-flight effects are included in the analysis. As a result, the energy analysis in Section IV is a time-averaged approximation as are the magnitudes of the energy losses.

VII. Conclusions

The best transport results were obtained with the large diameter channel. In this channel, transport efficiencies ranging from 33% to 100% were deduced from this analysis. Total proton currents of a few hundred kiloamperes of 1-MeV protons were calculated to be transported a distance of one meter. There is a trade off between proton current and transport efficiency in the interpretation of these measurements. For 100% transport efficiency in the shots analyzed, the current is $\leq$ 250 kA, but for the smallest transport efficiency (33%) of any of the shots, the current is 300 kA. Energy losses within the transport channel were less than 15% of the maximum proton energy.

References

1. G. Cooperstein, S. A. Goldstein, D. Mosher, R. J. Barker, J. R. Boller, D. G. Colombant, A. Drobot, R. A. Meger, W. F. Oliphant, P. F. Ottinger, F. L. Sandel, S. J. Stephanakis and F. C. Young, "NRL Light Ion Beam Research for Inertial Confinement Fusion," 5th Workshop on Laser Interaction and Related Plasma Phenomena, Rochester, N.Y., 1979.

2. F. L. Sandel, F. C. Young, S. J. Stephanakis, W. F. Oliphant, G. Cooperstein, S. A. Goldstein, and D. Mosher, Bull. Am. Phys. Soc. 24, 1031 (1979); and F. C. Young, F. L. Sandel, S. J. Stephanakis, P. G. Blauner, W. F. Oliphant, G. Cooperstein, S. A. Goldstein and D. Mosher, ibid. 24, 1031 (1979).

3. D. Mosher, G. Cooperstein, S. A. Goldstein, D. G. Colombant, P. F. Ottinger, F. L. Sandel, S. J. Stephanakis and F. C. Young, "Transport and Bunching of Light Ion Beams for Pellet Fusion," 3rd Inter. Conf. on High Power Electron and Ion Beam Res. and Tech., Novosibirsk, USSR, 1979.

4. J. Golden, R. A. Mahaffey, J. A. Pasour, F. C. Young, C. A. Kapetanakos, Rev. Sci. Instrum. 49, 1384 (1978).

5. D. Mosher, G. Cooperstein, S. J. Stephanakis, S. A. Goldstein, D. G. Colombant and R. Lee, "Intense Focussed Ion Beams and Their Interaction with Matter," 2nd Int. Conf. on High Power Electron and Ion Beam Res. and Tech., Cornell University, Ithaca, N.Y., 1977, p. 257; and S. A. Goldstein, G. Cooperstein, R. Lee, D. Mosher and S. J. Stephanakis, Phys. Rev. Lett. 40, 1504 (1978).

6. F. C. Young, F. Oliphant, S. J. Stephanakis, and A. K. Knudson, "Absolute Calibration of a Prompt Gamma Ray Detector for Intense Bursts of Protons," NRL Memorandum Report 4171, March, 1980.

7. D. G. Colombant and S. A. Goldstein, "Scaling Laws for Ion Beam Losses in Plasma Channels," Conf. Record-1980 IEEE Inter. Conf. on Plasma Science, Madison Wisconsin, 1980, p. 37.

8. P. F. Ottinger, D. Mosher and Shyke A. Goldstein, Phys. Fluids 22, 332 (1979).

9. S. A. Goldstein and D. A. Tidman, "Particle Beam Acceleration in Magnetized Moving Plasma," Conf. Record-1980 IEEE Inter. Conf. on Plasma Science, Madison, Wisconsin, 1980, p. 96.

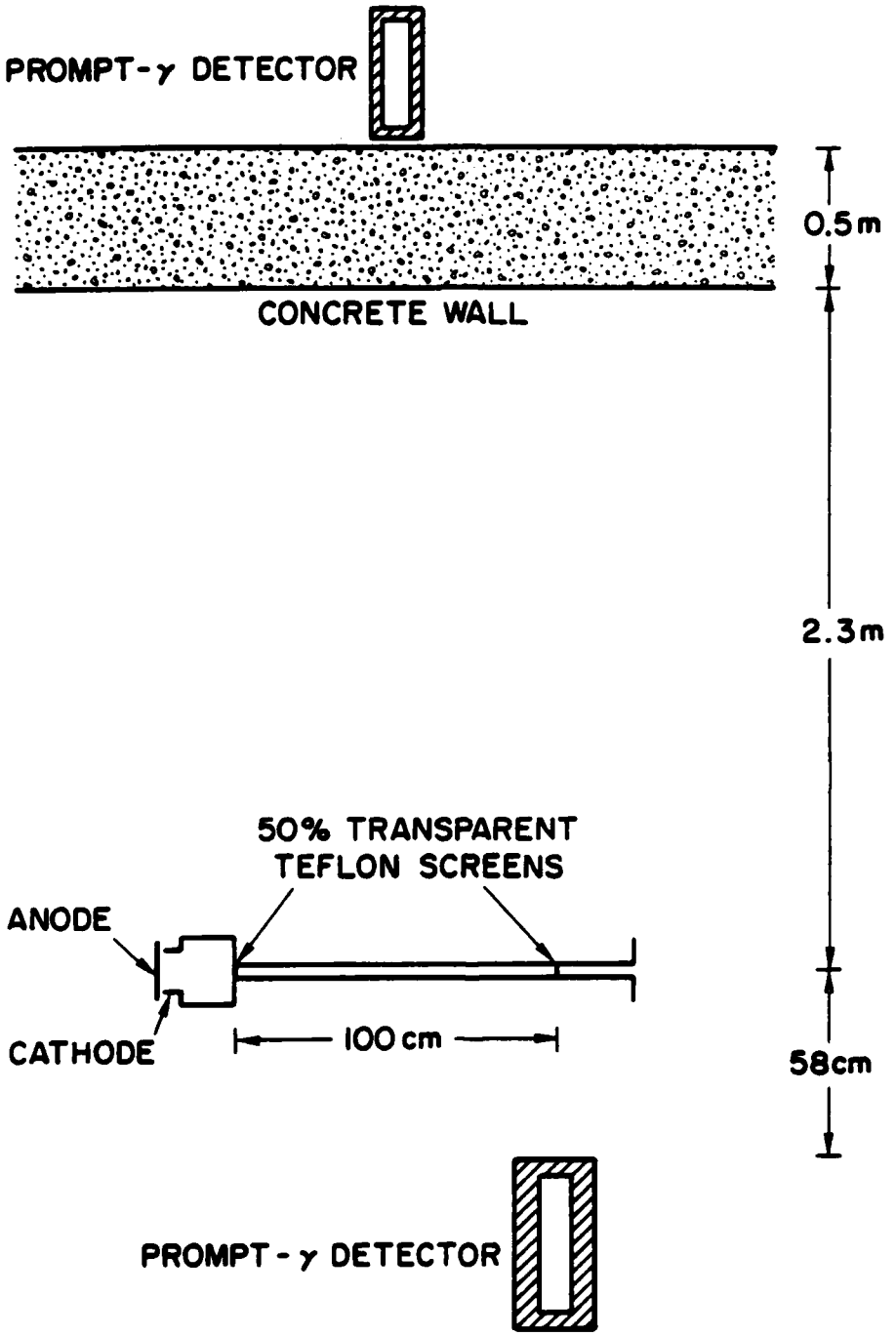

Fig. 1 — Experimental arrangement of the prompt-gamma detectors for the transport experiments.

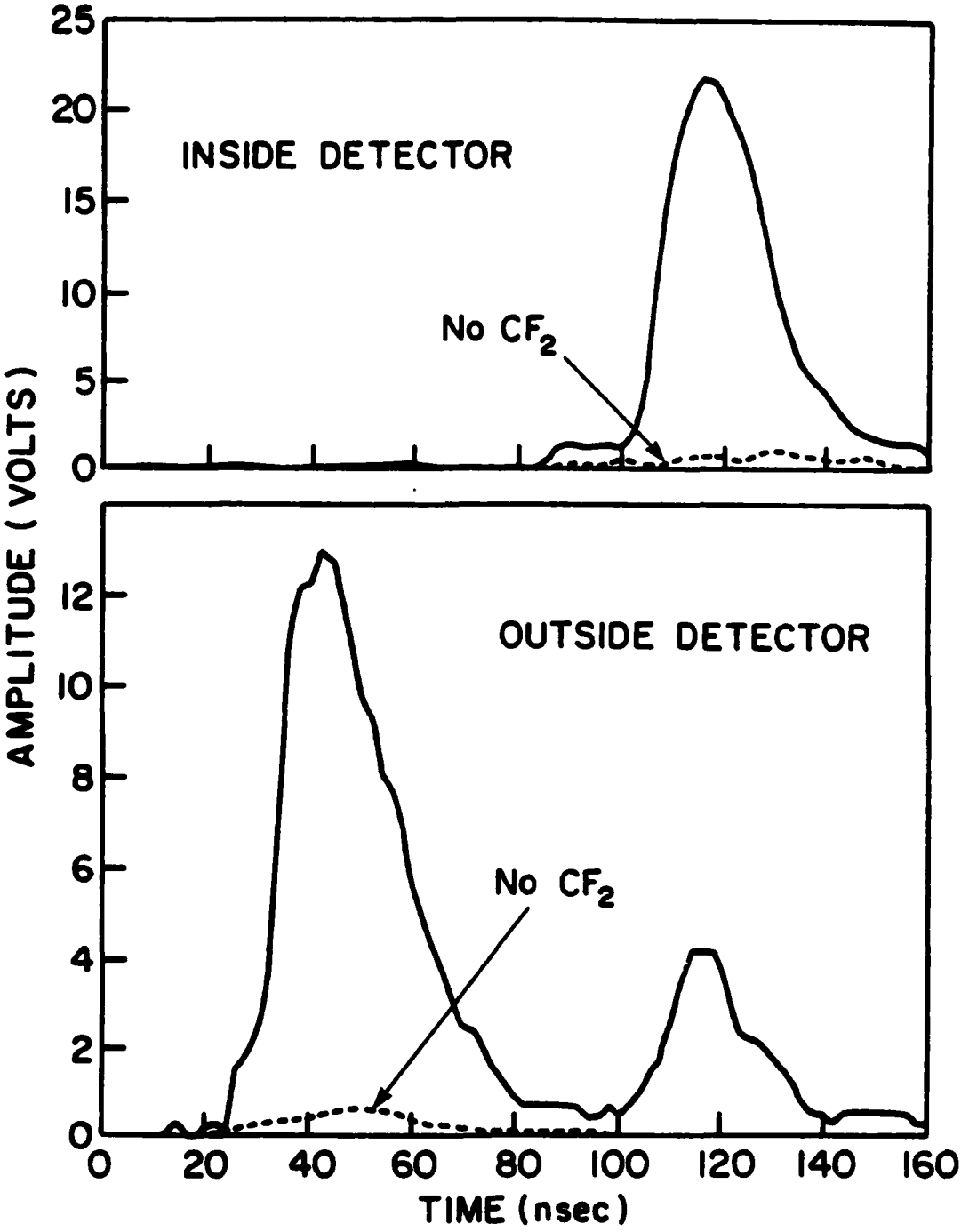

Fig. 2 — Measured traces from the prompt-gamma detectors for Shot 412 with Teflon targets (solid line) and for Shot 411 without Teflon targets (dashed line).

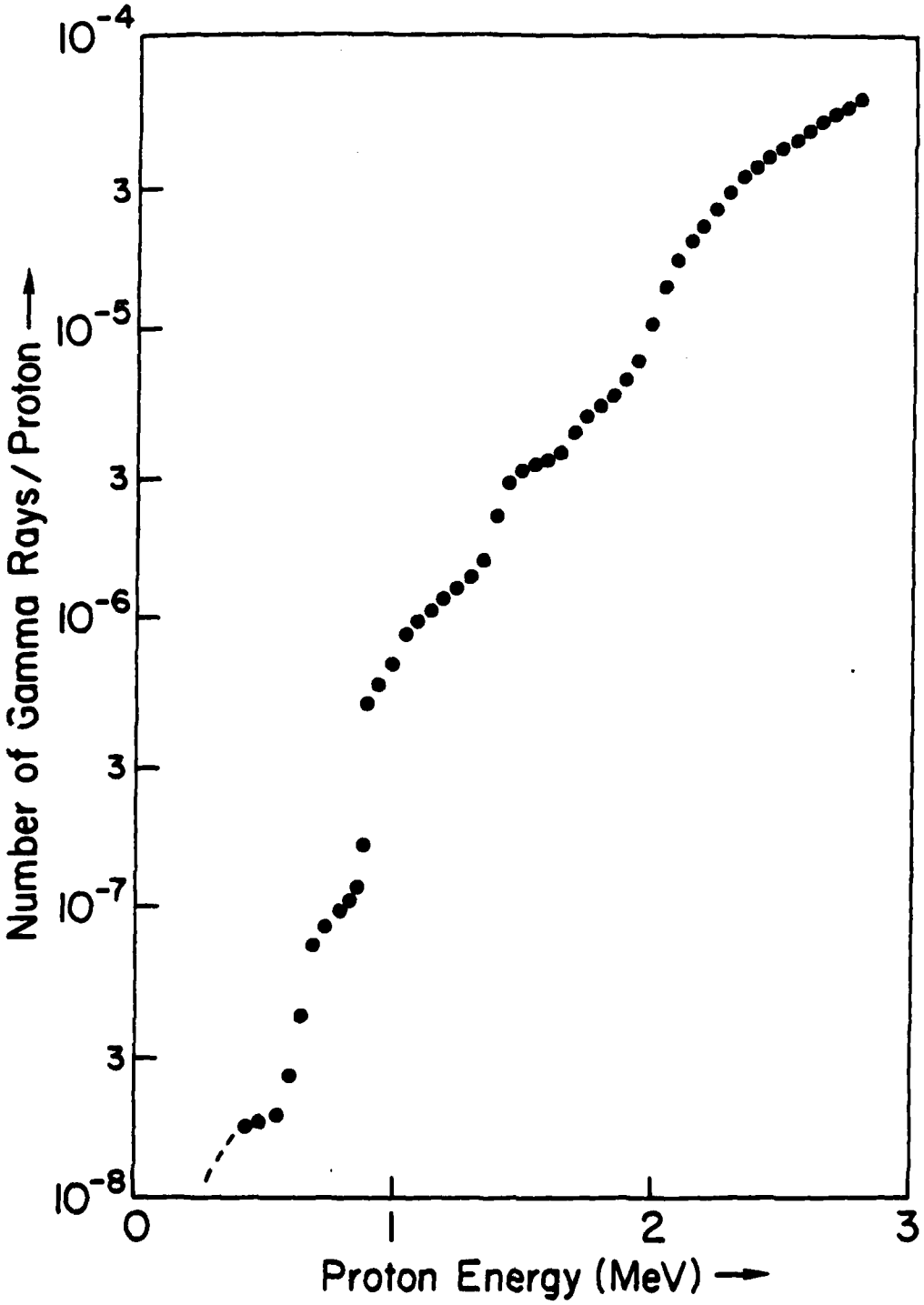

Fig. 3 — Measured thick-target yield for the $^{19}F(p,\alpha\gamma)^{16}O$ reaction on a Teflon target.

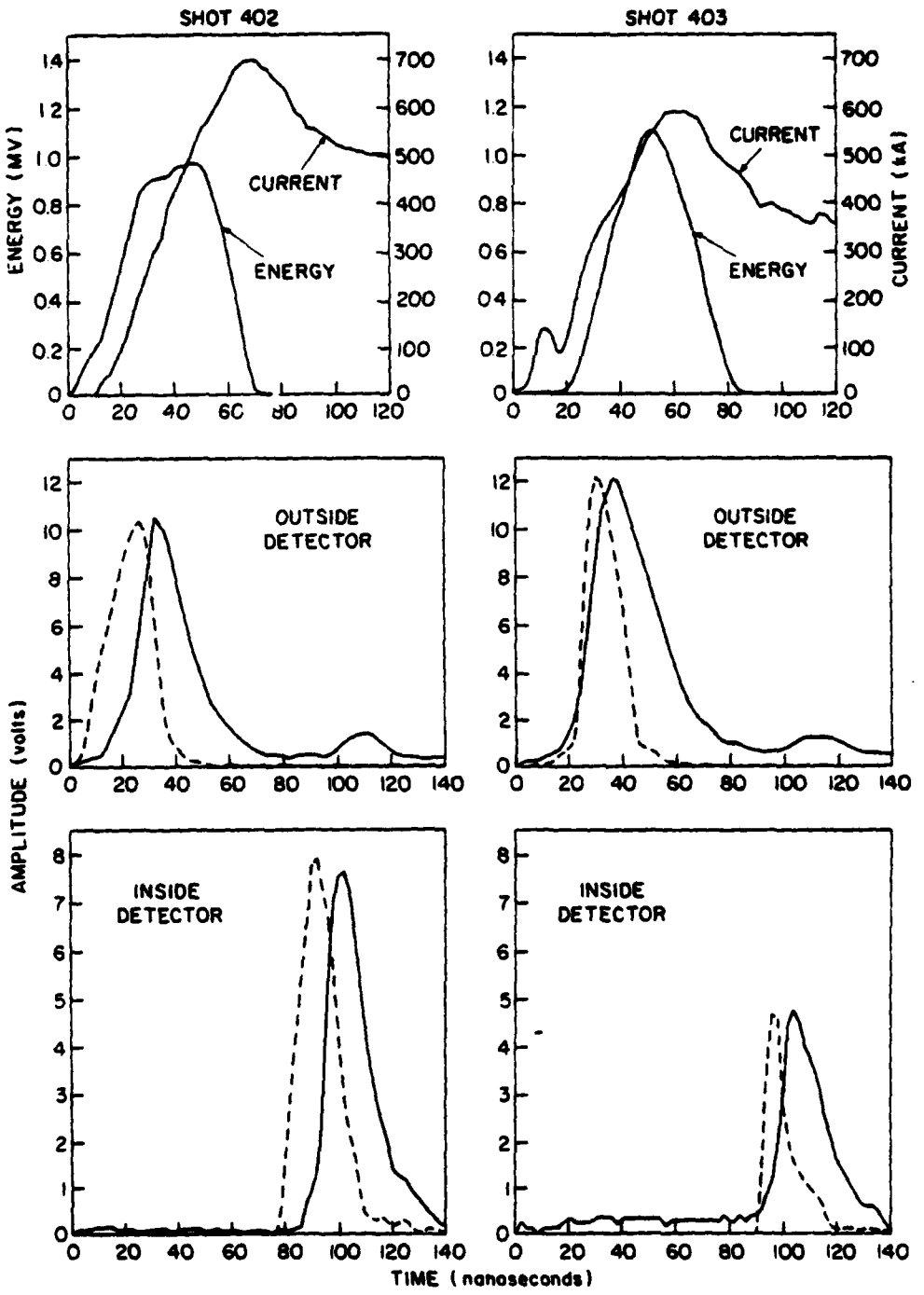

Fig. 4(a) — A comparison of measured (solid line) and calculated (dashed line) prompt-gamma responses for Shots 402 and 403 with the large diameter transport channel. The calculated responses are normalized in amplitude to the measured signals. Also, the proton energy and current which were used to calculate the prompt-gamma responses are displayed. No energy losses are included in these calculations.

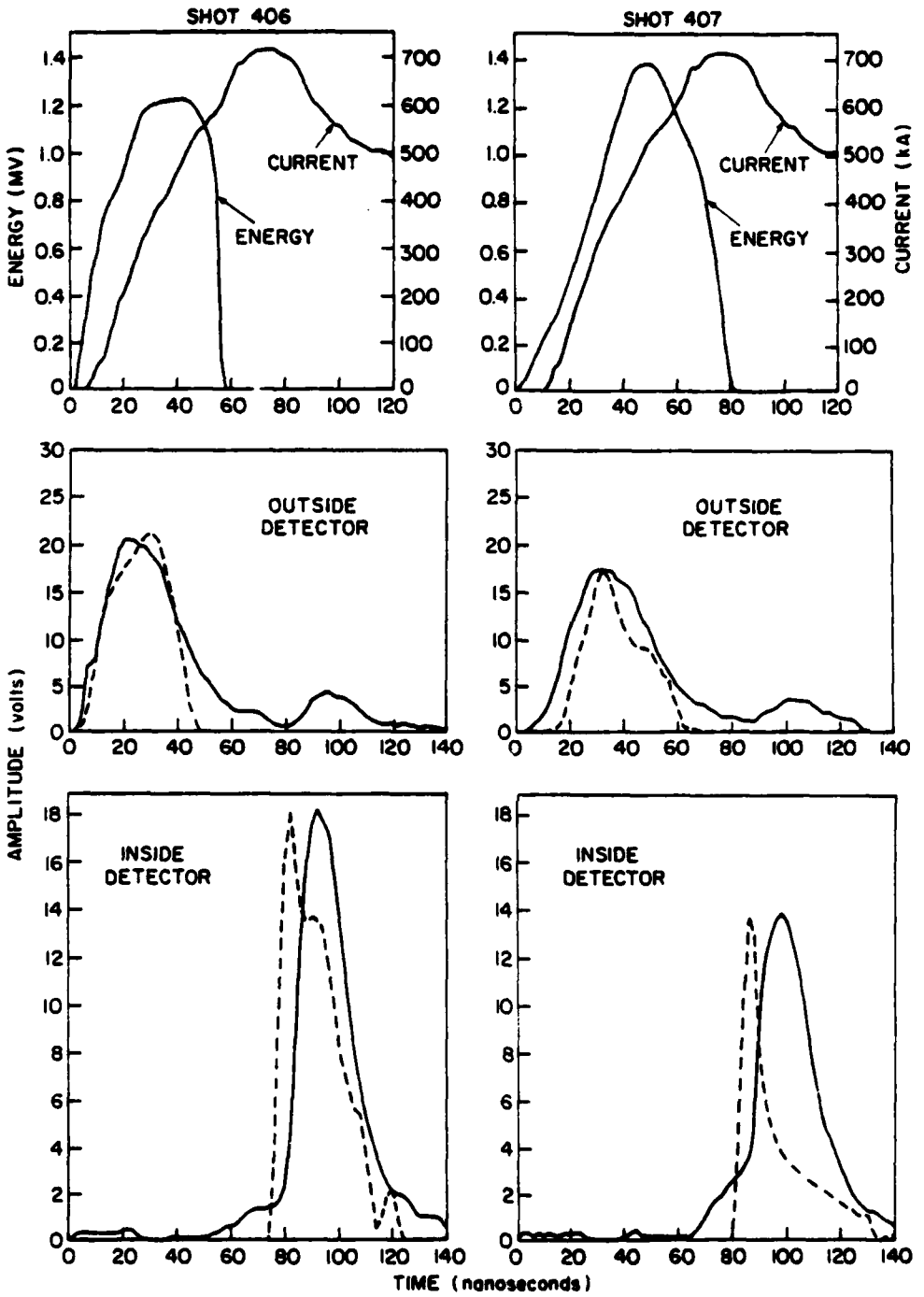

Fig. 4(b) — A comparison of measured (solid line) and calculated (dashed line) prompt-gamma responses for Shots 406 and 407 with the large diameter transport channel. The calculated responses are normalized in amplitude to the measured signals. Also, the proton energy and current which were used to calculate the prompt-gamma responses are displayed. No energy losses are included in these calculations.

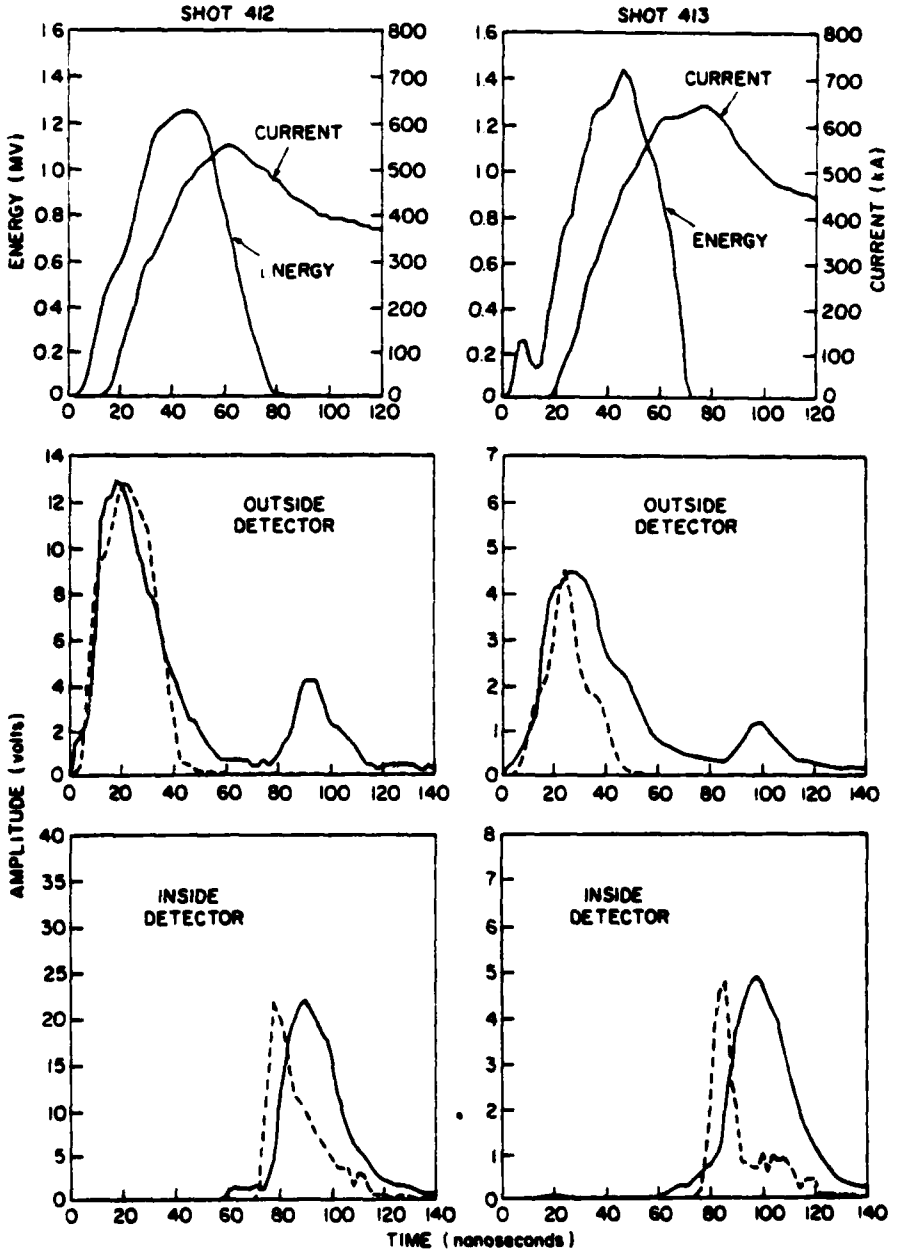

Fig. 4(c) — A comparison of measured (solid line) and calculated (dashed line) prompt-gamma responses for Shots 412 and 413 with the large diameter transport channel. The calculated responses are normalized in amplitude to the measured signals. Also, the proton energy and current which were used to calculate the prompt-gamma responses are displayed. No energy losses are included in these calculations.

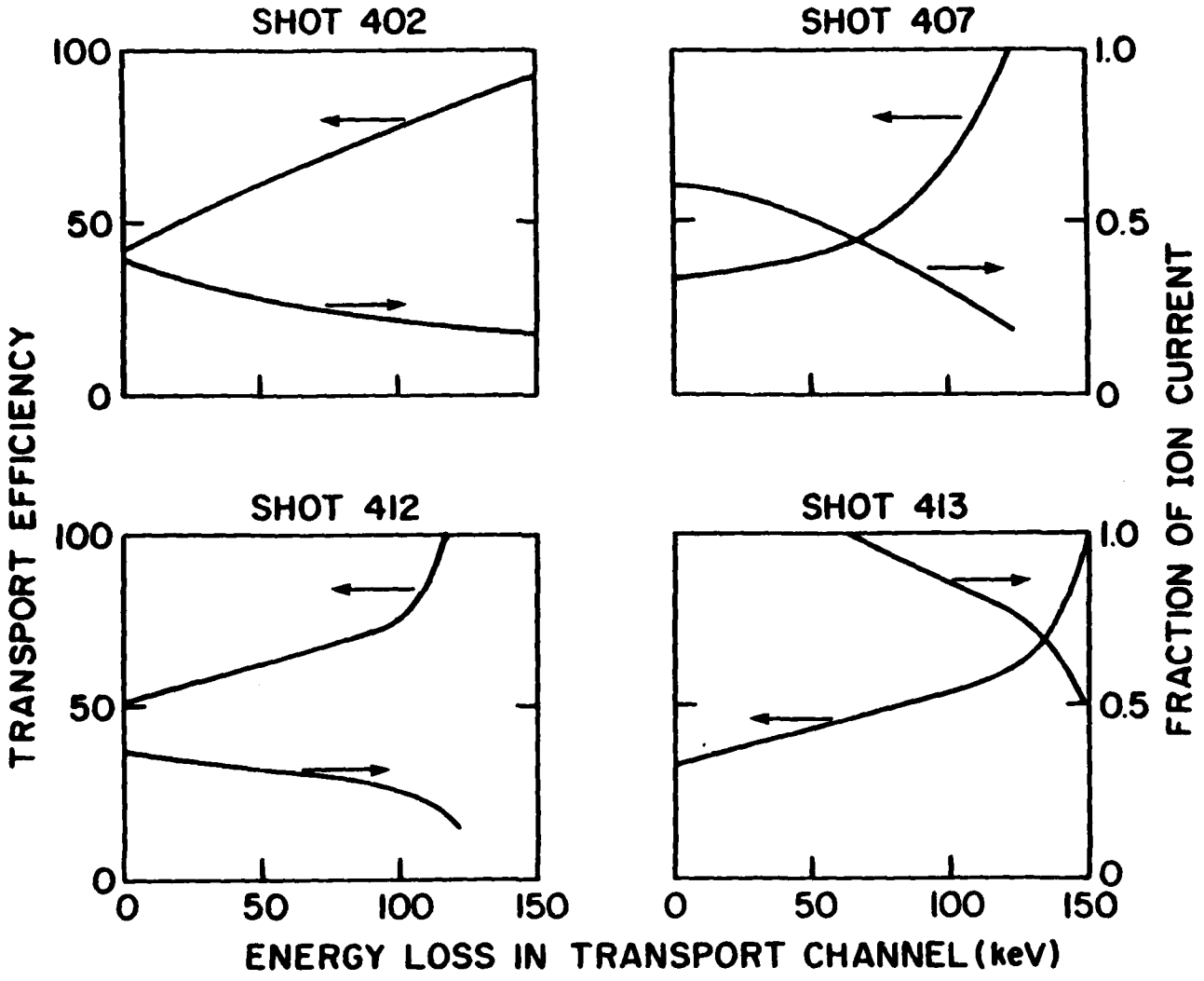

Fig. 5 — Transport efficiencies determined with energy loss included in the analysis. The fraction of ion current required to fit the magnitude of the prompt-gamma response is also given as a function of the energy loss in the transport channel.

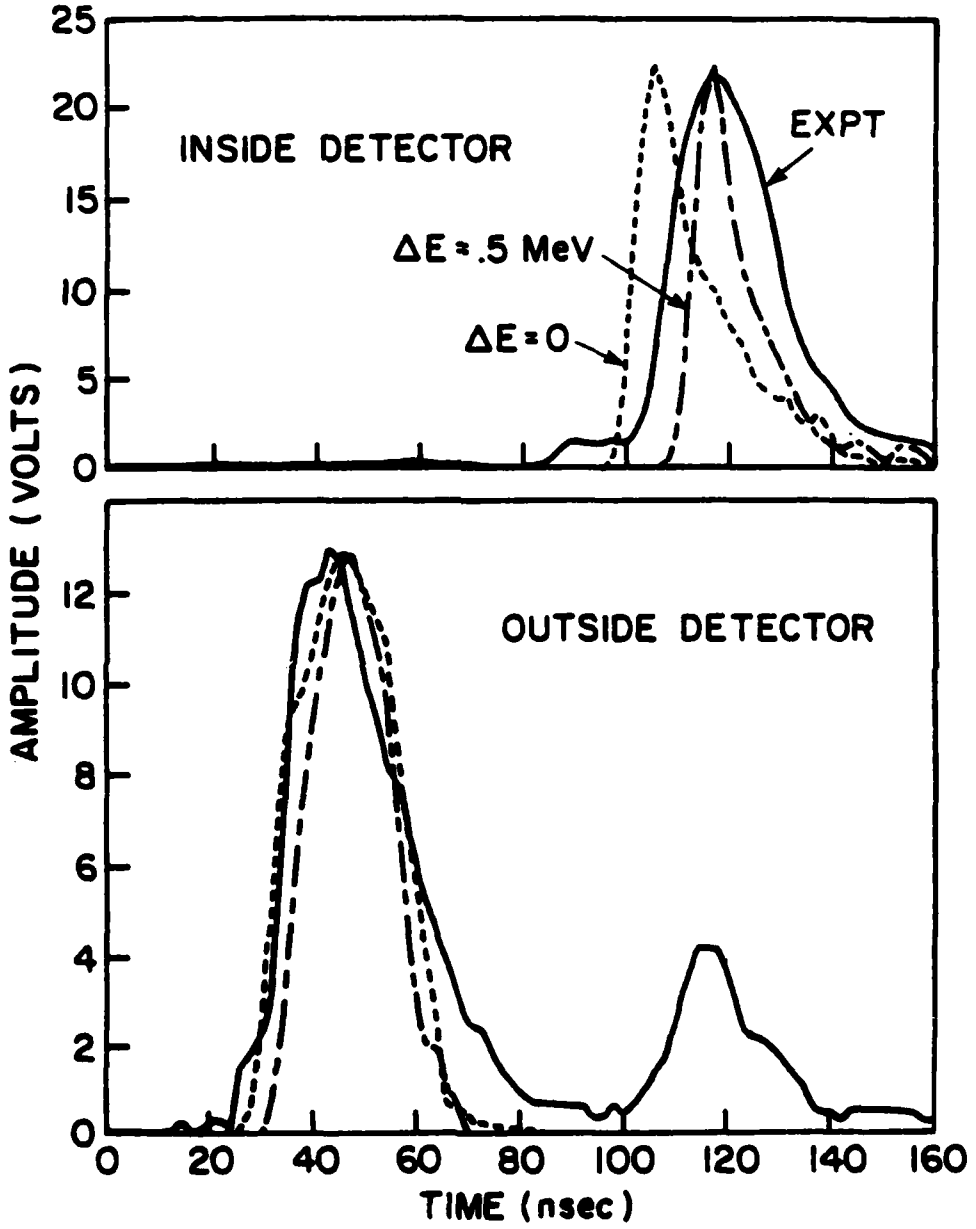

Fig. 6 — A comparison of measured (solid line) and calculated prompt-gamma responses without energy loss (short dashed line) and with 500-keV energy loss (short-long dashed line) for both prompt-gamma detectors. The measured traces correspond to Shot 412.

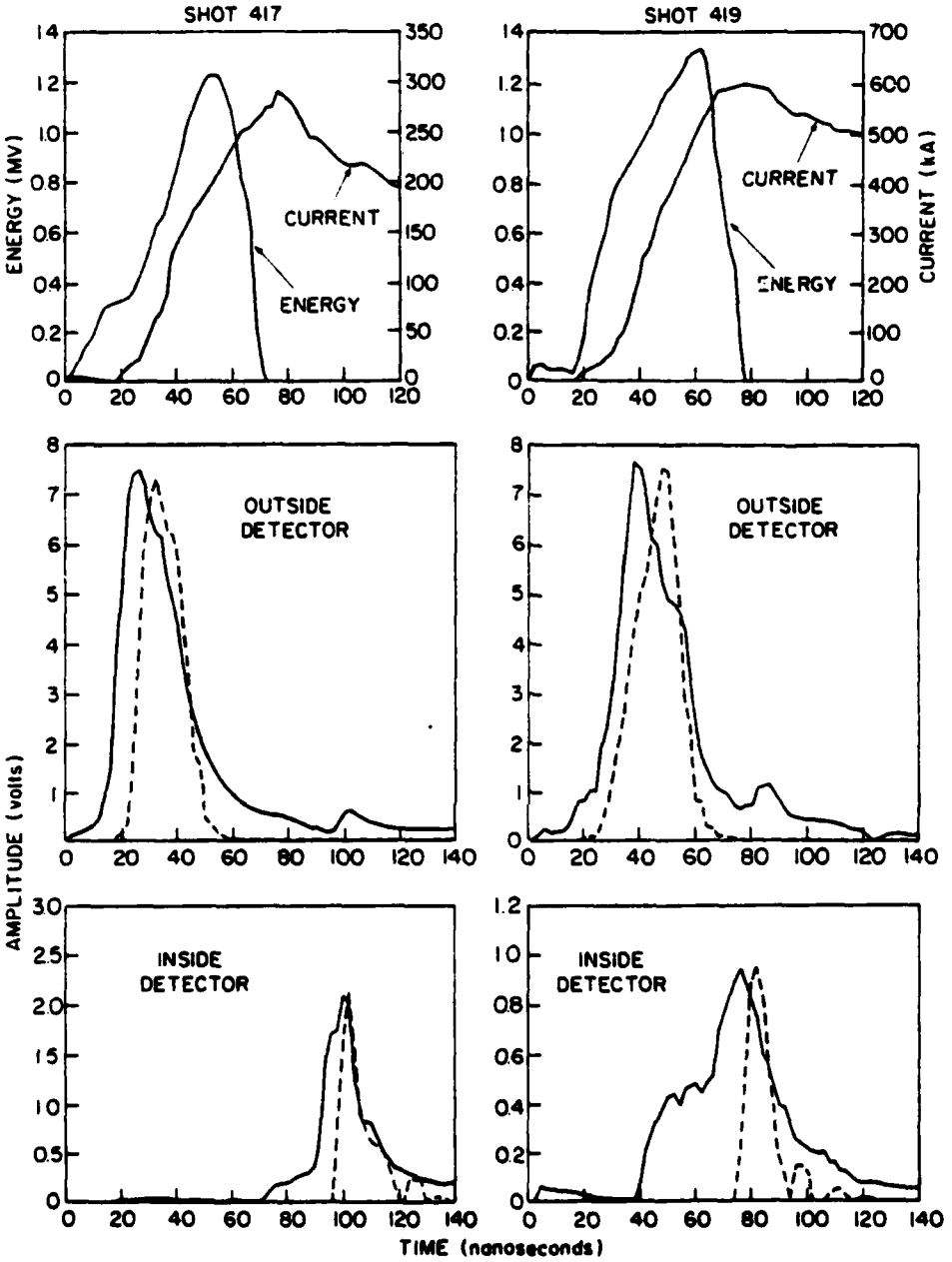

Fig. 7 — A comparison of measured (solid line) and calculated (dashed line) prompt-gamma responses for the small diameter transport channel (Shots 417 and 419). The proton energy and current which were used to calculate the prompt-gamma responses are also displayed. The calculated responses are normalized in amplitude to the measured signals. No energy losses were included in these calculations.

PART C

ABSTRACTS OF RELEVANT PAPERS

Abstract Submitted
For the Twenty-first Annual Meeting
Division of Plasma Physics
November 12 to 16, 1979

Subject Category Number 4.3

Ion Beam Transport in Plasma Channels.*

F. L. SANDEL†, F. C. YOUNG, S. J. STEPHANAKIS, F. W. OLIPHANT, G. COOPERSTEIN, SHYKE A. GOLDSTEIN†, and D. MOSHER, Naval Research Laboratory--Intense proton beams produced in the GAMBLE II generator have been efficiently transported over distances greater than one meter in wall-stabilized current-carrying plasma channels. Ion beams are allowed to ballistically focus in a neutral gas background so that a fully current neutralized beam is injected into the plasma channel, which begins at the ion focus. Channel diameters of 1.6 cm and 4.5 cm have been studied with channel gas pressures in the range .2-2 Torr. Efficient transport has been observed except above a well defined channel current in the 1.6 cm channel, indicating possible instability. The primary diagnostic has been the observation of gamma rays from nuclear reactions in fluorine targets. The detailed analysis of these data will be presented in the following paper. Continuing experiments will be discussed.

*Work supported by the Department of Energy.
†JAYCOR, Inc., Alexandria, VA 22304

( ) Prefer Poster Session

(X) Prefer Oral Session

( ) No Preference

(X) Special Requests for placement of this abstract: See Below

(Special Facilities Requested (e.g., movie projector)

Submitted by:

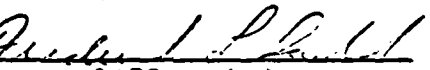
(signature of APS member)

F. L. Sandel
(same name typewritten)
JAYCOR, Inc.
205 S. Whiting St.
Alexandria, VA 22304
(address)

This form, or a reasonable facsimile, plus *Two Xerox Copies* must be received NOT LATER THAN FRIDAY, AUGUST 17, 1979 at the following address:

Division of Plasma Physics Annual Meeting
Mrs. Marianne Weissenburger
Plasma Physics Laboratory
P.O. Box 451
Princeton, N.J. 08540

This abstract should precede "Analysis of Proton Transport Experiment with a Prompt Gamma Diagnostic", F. C. Young, et. al.

Sandel

Abstract Submitted
For the Twenty-first Annual Meeting
Division of Plasma Physics
November 12 to 16, 1979

Subject Category Number 4.3 Non-relativistic Ion Beams

Analysis of Proton Transport Experiments with a Prompt Gamma Diagnostic.* F. C. YOUNG, F. L. SANDEL†, S. J. STEPHANAKIS, P. G. BLAUNER†, F. W. OLIPHANT, G. COOPERSTEIN, S. A. GOLDSTEIN†, and D. MOSHER, Naval Research Laboratory.--The time variation of the current of intense bursts of protons has been determined by detecting prompt gamma rays from the $^{19}F(p,\alpha\gamma)^{16}O$ reaction. Detectors have been absolutely calibrated to measure Amperes of protons provided the proton energy is known. Measurements with this diagnostic on the transport experiments described in the previous talk were analyzed to evaluate proton currents and transport efficiencies. The dependence of these measurements on proton energy losses due to resistive and inductive effects in the diode and proton deceleration due to the return current eiectric field will be discussed. For energy losses of a few hundred keV, peak proton currents of ~0.3 MA are focussed and transported 1 meter with ~50% efficiency.

*Work supported by the Department of Energy
†JAYCOR, Inc., Alexandria, VA 22304

( ) Prefer Poster Session

(X) Prefer Oral Session

( ) No Preference

(X) Special Requests for placement of this abstract:

( ) Special Facilities Requested (e.g., movie projector)

Submitted by:

Frank C. Young
(signature of APS member)

Frank C. Young
(same name typewritten)
Code 6770
Naval Research Laboratory
(address) Washington, D.C. 20375

This form, or a reasonable facsimile, plus *Two Xerox Copies* must be received NOT LATER THAN FRIDAY, AUGUST 17, 1979 at the following address:

Division of Plasma Physics Annual Meeting
Mrs. Marianne Weissenburger
Plasma Physics Laboratory
P.O. Box 451
Princeton, N.J. 08540

It is requested that this abstract follow the abstract entitled "Ion Beam Transport in Plasma Channels" by F. L. Sandel, et. al.

INTERNATIONAL ATOMIC ENERGY AGENCY

8th INTERNATIONAL CONFERENCE ON PLASMA PHYSICS
AND CONTROLLED NUCLEAR FUSION RESEARCH

Brussels, 1–10 July 1980

IAEA-CN-38/ P-2

PROGRESS AT NRL AND CORNELL IN LIGHT-ION-BEAM RESEARCH FOR ICF†

G. Cooperstein, Shyke A. Goldstein*, D. Mosher,

R. J. Barker*, J. R. Boller, D. G. Colombant, A. Drobot**,

R. A. Meger*, W. F. Oliphant, P. F. Ottinger*, F. L. Sandel*,

S. J. Stephanakis and F. C. Young

Naval Research Laboratory, Washington, DC 20375, USA

G. Ginet, D. A. Hammer, S. Humphries, Jr.***, J. M. Neri,

R. Pal and R. N. Sudan

Laboratory of Plasma Studies

Cornell University, Ithaca, NY 14853, USA

ABSTRACT

Proof-of-principle and scaling experiments for light-ion-driven inertial-confinement fusion are in progress at NRL. Important advances have been made in the area of ion production with pinch-reflex diodes and in the areas of beam focusing and transport. At Cornell, light-ion beams of Li^{+1}, B^{+1} and C^{+1} have been produced and work on producing low divergence ion beams has progressed.

1. INTRODUCTION

Proof-of-principle and scaling experiments for light-ion-driven inertial-confinement fusion are in progress using generators which are appropriate for use as ignition-system modules. Intense beams extracted from ion diodes already have particle energies, currents and pulse durations which could satisfy system requirements related to ion production, focusing, and transport to an ICF target [1]. Recent results in light-ion-beam research at NRL and Cornell are summarized below.

At NRL, important advances have been made in the area of ion production with pinch-reflex diodes, and in the areas of beam focusing and transport. These advances include the following: (1) production of ≥ 100 kJ proton beams and deuteron beams with peak ion powers approaching 2 TW on the PITHON generator in collaboration with Physics International Co., (2) production of 60 kA of protons at 5 MeV with a 25 ohm ion diode on the AURORA accelerator in collaboration with Harry Diamond Laboratories (HDL), (3) focusing of 0.5 TW deuteron beams produced on the NRL GAMBLE II generator to current densities of about 300 kA/cm^2, and (4) efficient transport of 100 kA-level ion beams over 1-meter distances using Z-discharge plasma channels.

At Cornell, advances have been made in the production of light-ion beams other than protons. Beams consisting of Li^{+1},

Presented at the Fifth Workshop on
"Laser Interaction and Related Plasma Phenomena"
held at the Laboratory for Laser Energetics
Rochester, New York, November 5-9, 1979

NRL LIGHT ION BEAM RESEARCH FOR INERTIAL CONFINEMENT FUSION†

G. Cooperstein, Shyke A. Goldstein*, D. Mosher
R. J. Barker*, J. R. Boller, D. G. Colombant,
A. Drobot**, R. A. Meger*, W. F. Oliphant,
P. F. Ottinger*, F. L. Sandel*, S. J. Stephanakis,
and F. C. Young

Naval Research Laboratory
Washington, DC 20375

ABSTRACT

There is presently great interest in using light ion beams to drive thermonuclear pellets. Terrawatt-level ion beams have been efficiently produced using conventional pulsed power generators at Sandia Laboratory with magnetically-insulated ion diodes and at the Naval Research Laboratory with pinch-reflex ion diodes. Both laboratories have recently focused ion beams to pellet dimensions. This paper reviews recent advances made at NRL in the area of ion production with pinch-reflex diodes, and in the areas of beam focusing and transport. In addition, modular generator and beam requirements for pellet ignition systems are reviewed and compared with the latest experimental results. These results include the following: (1) production of ≥ 100 kJ proton and deuteron beams with peak ion powers approaching 2 TW on the PITHON generator in collaboration with Physics International Co., (2) focusing of 0.5 TW deuteron beams produced on the NRL Gamble II generator to current densities of about 300 kA/cm^2, and (3) efficient transport of 100 kA level ion beams over 1 meter distances using Z-discharge plasma channels.

† Work supported by Defense Nuclear Agency, Washington, DC 20305 and Department of Energy, Washington, DC 20545
* JAYCOR, 205 S. Whiting Street, Suite 500, Alexandria, VA 22304
** Science Applications, Inc., 8400 Westpark Dr., McLean, VA 22101

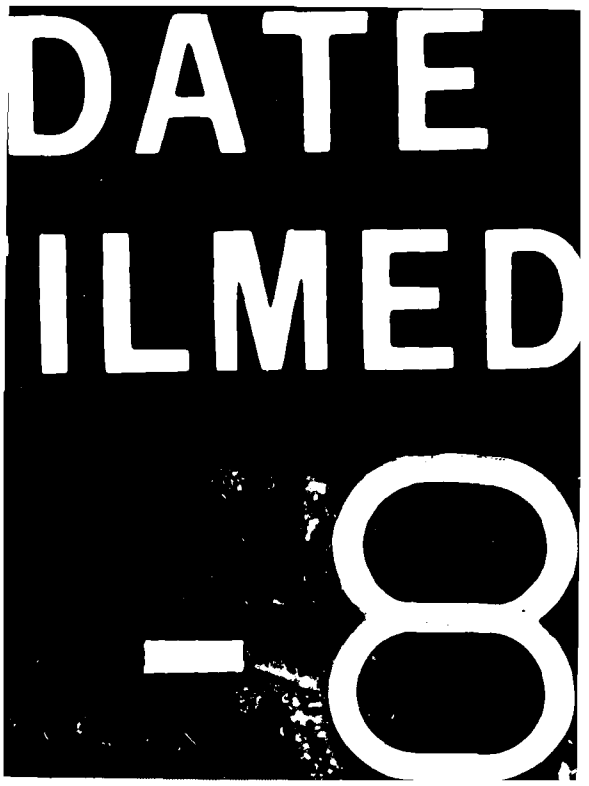
DATE
ILMED
-8